IEEE Access
Multidisciplinary | Rapid Review | Open Access Journal

IEEE POWER & ENERGY SOCIETY SECTION

Received May 11, 2021, accepted May 27, 2021, date of publication June 2, 2021, date of current version June 9, 2021.

Digital Object Identifier 10.1109/ACCESS.2021.3085173

New Analysis Framework of Lyapunov-Based Stability for Hybrid Wind Farm Equipped With FRT: A Case Study of Egyptian Grid Code

AHMED A. SALEM[1], AZZA A. ELDESOUKY[2], AHMED A. FARAHAT[2], AND ABDELAZEEM A. ABDELSALAM[1], (Member, IEEE)

[1]Electrical Engineering Department, Faculty of Engineering, Suez Canal University, Ismailia 41522, Egypt
[2]Department of Electrical Engineering, Faculty of Engineering, Port Said University, Port Fouad 42526, Egypt

Corresponding author: Ahmed A. Salem (ahmed_salem@eng.suez.edu.eg)

ABSTRACT Due to the continuous increase of fuel prices and pollutions, the use of renewable energy especially wind has increased. In developing countries including Egypt, squirrel cage induction generator wind turbine (SCIG- WT) represents a considerable proportion of the total capacity of installed wind farm due to its qualities such as low cost and easy availability. However, its operation has a substantial effect on system stability. In contrast, doubly fed induction generator wind turbine (DFIG-WT) is broadly penetrated the electrical grid as it keeps the system stable. In this work, the ability of WT generators to continue operating rather than tripping at the time of faults is analyzed for proper stability investigation. The detailed control and stability of a grid-connected large scale SCIG and DFIG of Zafarana, Suez Gulf area, Egypt are discussed whereas the parameters of fault ride through (FRT) curve of Egypt grid code is utilized. Moreover, a precise analytical stability argument using a proposed integrated nonlinear dynamical model is presented. Conditions for global asymptotic stability of the SCIG in the sense of Lyapunov function (LF) are given and tested by time domain simulation. The eigenvalues of the matrices of LF and its derivative are determined by which the stability boundaries are determined depending on the positivity of these matrices. The dynamic behavior of the whole system is simulated in MATLAB/ Simulink interface programming while the practical data are collected from an experimental model consisting of DFIG-WT to demonstrate the efficacy of the FRT control system.

INDEX TERMS Egyptian grid code, eigenvalues, fault-ride through, Lyapunov theory, stability, wind generation.

I. INTRODUCTION

Different countries are intensifying the use of renewable energy for electrical power generation because of their numerous benefits. The wind power has received the most attention among variety of renewable energy resources [1]. Even though today's wind turbine (WT) generators are mostly doubly fed induction generators (DFIGs) [2], a considerable proportion of the existing WTs are still of the squirrel cage induction generator-based wind turbine (SCIG-WT) [3]. Furthermore, SCIGs-WT life extension programs are already underway, where WTs are refurbished to stretch their operational life to up to 30 years [4], [5]. Therefore, SCIGs-WT is continuing to attract the commercial interest for the coming 10-15 years [6]. However, due to the SCIG-WT's direct connection to the grid, it is vulnerable to grid voltage disruptions. Furthermore, the rotor deviates from the synchronous speed resulting in a significant amount of reactive power consumption at the stator terminals, further degrading grid voltage post fault recovery [6], [7]. Therefore, appropriate methods to analyze the stability of the SCIG-WT were presented [7]. Flexible AC transmission system (FACTS), rotor circuit control and braking resistors are three methods were used for improving induction generators (IGs) stability [6]–[8]. A method for improving the wind farm performance was investigated in [9]. This method was relied on the construction of combined wind farm composed of an equal number of DFIGs and SCIGs with the use of FACTS devices.

With the penetration of large capacity wind power, it is critical that the generators remain connected to the grid

The associate editor coordinating the review of this manuscript and approving it for publication was Dragan Jovcic.

during transient disturbances to maintain grid stability, which is referred to as fault ride-through (FRT) [10]. Many literature studies [7]–[14] have shown that WTs equipped with FRT can achieve safe operation without compromising the poor grid's stability.

One of the most used techniques for studying the non-linear stability of electrical systems is the Lyapunov-based stability technique. It focuses on a comparison of the transient energy at fault clearing time with the critical energy. The fundamental idea behind Lyapunov-based techniques is that any physical system contains an energy with a positive value that can be represented by an energy function (EF) [15]. If and only if the system's energy is positive and its energy derivative with respect to (w.r.t.) time is not positive, the system is stable. Otherwise, the system may become unstable [15], [16]. Numerous attempts have been made to define the system EF although there is no direct way to define it. In [16], EF has been used to ensure the system's stability when two separate WTs were connected to a common grid. The Lyapunov stability theory was used to investigate the small-signal stability of the DFIG [17]. A Lyapunov approach based on non-linearized models was used to assess the high signal stability of virtual synchronous generator/inverter-interfaced distributed generators [18]. Using the adaptive dynamic programming algorithm, the Lyapunov method was used to validate the stability of the proposed maximum power point tracking (MPPT) controller in [19]. In [20], the artificial intelligence integrated fractional order control for a DFIG was proposed. Whereas the fractional order Lyapunov system was used to ensure the stability of the closed loop system.

The main goal of this work is to enhance the performance of the SCIG of Zafarana, Suez Gulf area, Egypt to achieve high level of stability. A clustered wind farm composed of DFIGs and SCIGs is utilized. The WT's FRT capability has been taken into account to keep the WT connected to the network during grid faults. Moreover, sufficient conditions for SCIG's stability using the Lyapunov theory of stability is conducted. To check the efficacy of the FRT control system, various case studies are considered. This work's main contributions can be summarized as:

- Conditions for global asymptotic stability using Lyapunov theory for SCIG-WTs is presented.
- The detailed control and stability of a grid-connected large scale SCIG and DFIG farm in Zafarana, Suez Gulf area, Egypt are performed.
- The parameters of FRT curve of Egypt grid code are utilized.
- Simulated and practical fault conditions are examined.

This paper is structured as follows. In section II, the system configuration is proposed. Section III illustrates control and power flow of DFIG whereas the principle of the proposed FRT is introduced. In section IV, the stability problem is studied whereas concept of IG stability and parametric analysis of Lyapunov-based stability of SCIG are proposed. The simulation results and case studies are discussed in section V including the results of practical fault conditions. Finally, in section VI, the conclusions are presented.

II. SYSTEM CONFIGURATION

Fig. 1 depicts the proposed hybrid wind farm that is connected with an existing system in Zafarana, Suez Gulf area, Egypt. This system is a part of the Egyptian network which connects the 220 kV Suez grid to the 220 kV Safaga grid. Zafarana is considered as one of Egypt's most interesting wind energy applications sites. It is situated in Egypt's Suez Gulf, on the east coast of the Red sea, between latitude angles of 32′ 36″ and longitude angle equal to 29′ 06″ [21]. The proposed hybrid wind farm consists of the following parts, as shown in Fig.1:

- 17 × 600 kW Nordex (N43-600 kW-three blade) SCIG-WT connected to a 50 Hz, 22 kV medium-voltage system by a separate (800 kVA, 0.69/22 kV) transformer [22]. This is tranche one from 'Danish' wind-farm.
- 12 × 850 kW Gamesa (G52-850 kW-three bladed) DFIG-WT connected to a 50 Hz, 22 kV medium-voltage system by a separate (1100 kVA, 0.69/22 kV) transformer [22].

The proposed hybrid wind farm is linked to the national grid through 6.5 km transmission line located north of the site at Zafarana substation (ZF1). The ZF1 is equipped with five transformers that link the entire wind farm in the region. Three of them have a rating of 125 MVA, 22/220 kV each, and the rest have a rating of 75 MVA [23]. The system parameters and WT modeling are listed in Appendices A and B, respectively.

The SCIG-WT is shown in Fig. 1, with the WT rotor coupled to the generator via a gear box and the stator connected to the grid via a two-winding transformer. To supply reactive power to a 3-phase IG, a capacitor bank is connected. Moreover, a simple layout of DFIG-WT with the control system and the power flow is conducted as shown in Fig.1. In DFIG-WT, the power generated from wind is transferred to the gird via two paths. The main path is the direct-connected stator link, whereas the secondary path is the rotor circuit which supplies the power via two back-to-back converters. Most of the power is transmitted via the stator and the rotor circuit and the converters only feed small portion. The control and power flow of DFIG are explained in the next section.

III. CONTROL AND POWER FLOW OF DFIG

The detailed decoupled control applied to DFIG d-q reference frame is explained in Fig.2. According to Fig.2, the behavior of DFIG is investigated for both normal operation (conventional control scheme) and fault operation (FRT scheme). In general, vector control techniques are used to control power converters that are made up of rotor side converter (RSC) and grid side converter (GSC) with a common dc-bus between them, as shown in Fig. 2. The RSC's objective is to control active and reactive power on the grid independently, while the GSC's goal is to maintain a constant

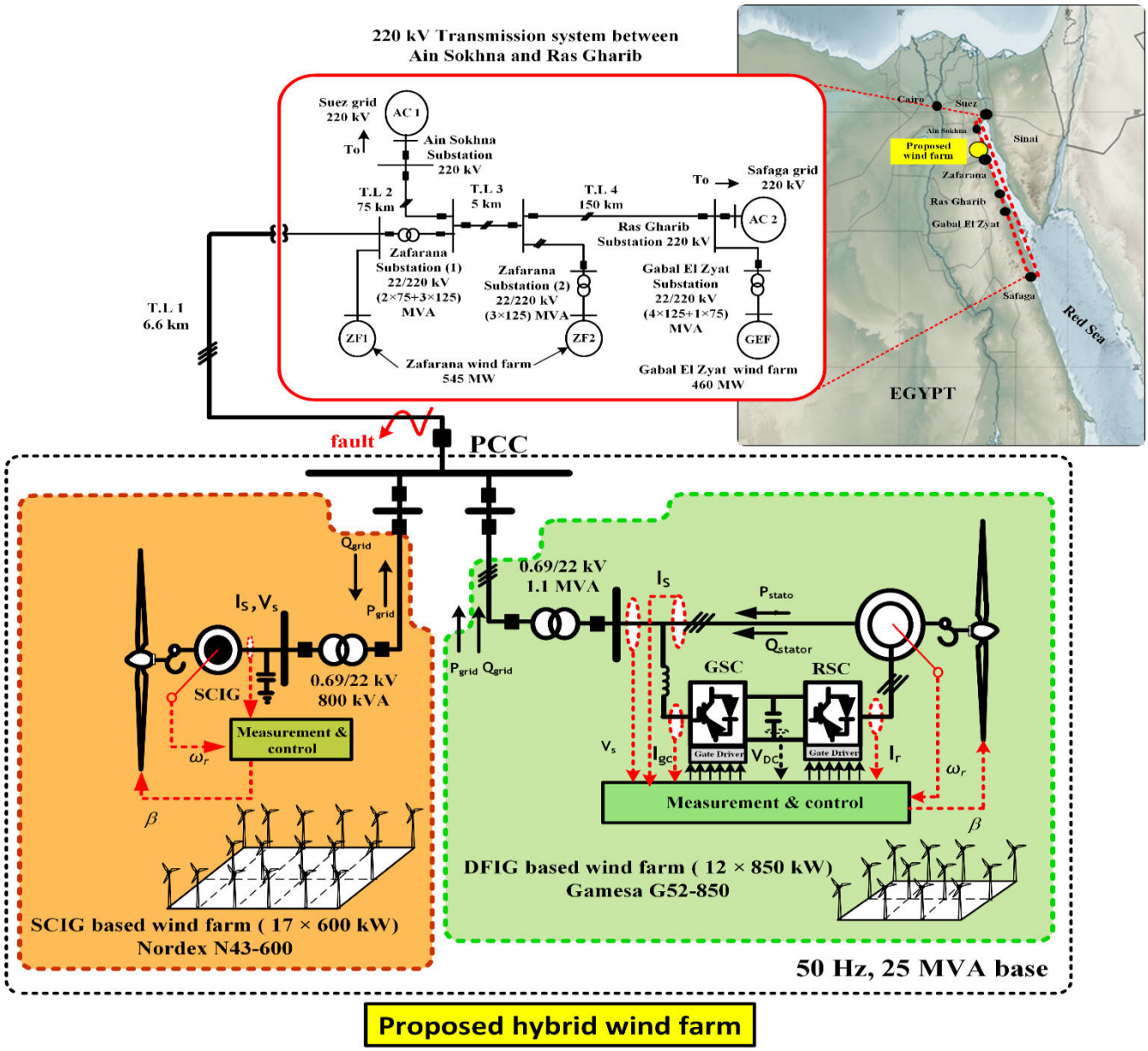

FIGURE 1. Schematic diagram of the proposed hybrid wind farm connected with utility grid.

dc-link capacitor voltage and to ensure converter operation with unity power factor [24]. The detailed model of the RSC and GSC are found in many published papers [24]–[29]. To synthesize the applied voltage on the RSC and GSC, two stage controllers are used. These are current and power controllers, respectively. In this paper, the set points of the second stage are depicted by two ways according to the state of operation (i.e., normal operation or fault operation). In normal operation the set points of the reactive power of RSC and GSC of the second stage can be set to zero. These set points are used in normal operation to reduce the losses and maximize the power transfer between the generator and the grid [24], [25].

However, at fault operation, a reactive current injection according to Egyptian grid code is conducted. The principle of the required reactive current for FRT is discussed in the next section.

To rapidly switch between the normal operation and FRT operation, it is critical to detect voltage dips quickly [30]. As shown in Fig.2, the fault detection method used is based on the instantaneous voltage measurement (V_{sd} and V_{sq}) to calculate the voltage error vector $|V_{error}|$ that indicates to the level of the voltage dip.

V_{ref} is set equal to the rated voltage. $|V_{error}|$ is compared with $V_{threshold}$ to detect the fault. The threshold voltage value is set 0.1 $|V_s|$ according to Egypt grid code requirement [31].

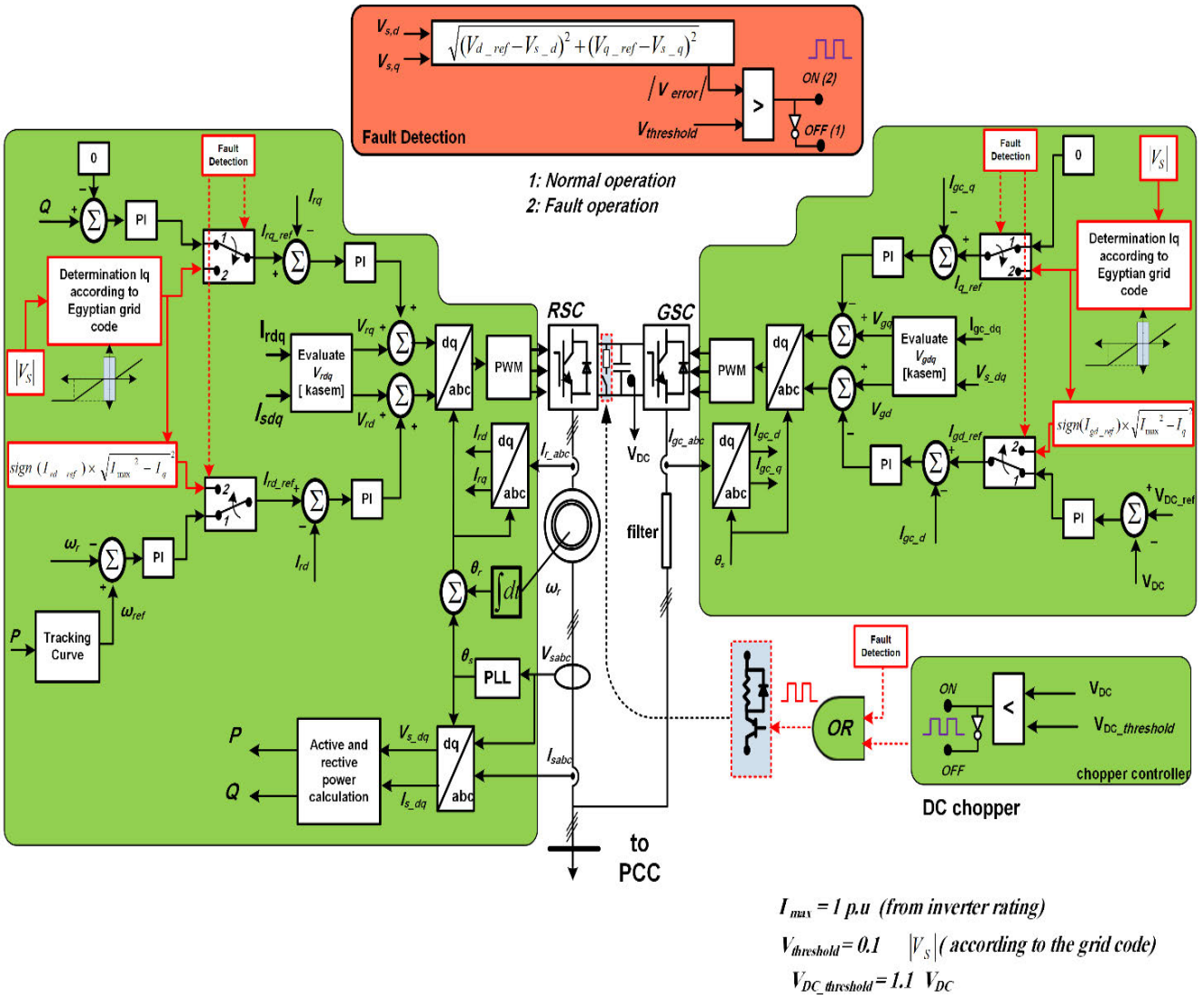

FIGURE 2. Schematic diagram of control and power flow of DFIG.

A. PRINCIPLE OF FRT BASED ON EGYPTIAN GRID CODE

Wind farms must be able to provide voltage support during and after fault based on specific voltage–time limits profiles recommended by modern grid codes. FRT stands for voltage–time profiles. For example, the German and Spanish grid codes specified dynamic voltage support during faults by injecting reactive current [32]. According to the wind farm grid connection code in Egypt, wind generators are not allowed to be disconnected from the grid in the event of temporary voltage dips [31]. Fig. 3 describes the FRT requirements for different countries including Egypt [29]–[33]. According to FRT requirements of Egypt, if the WT voltage profile remains ''0%'' of the nominal voltage for a period not exceed 150 ms, the WT must stay connected with the national grid [31].

The parameters of FRT curve for different countries, depending on their power system characteristics and the employed protection, have been listed in Table 1 [29], [34].

TABLE 1. Parameters of FRT curve for different countries.

Grid code	Voltage dip duration (ms)	Minimum PCC voltage (%)	Voltage restoration time (ms)
Germany	150	0	1500
Canada	150	0	1000
Egypt	150	0	3000
Spain	500	20	1000
USA	625	15	3000

The parameters of FRT curve for different countries, depending on their power system characteristics and the employed protection, have been listed in Table 1 [29], [34]. The wind generator must ensure the reactive current support. Fig. 4 depicts the dynamic voltage support's concept for wind farm that are connected to utility grid, as defined by Egyptian grid code [31].

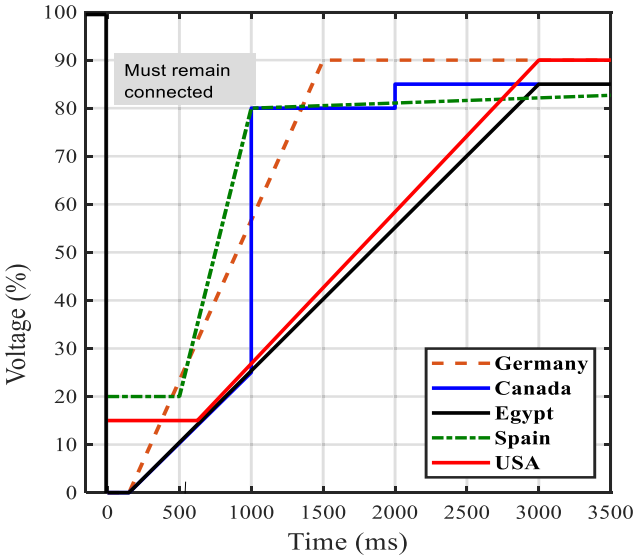

FIGURE 3. FRT requirements for different countries [29]–[33].

As shown in Fig.4 and according to (1), when the voltage dip occurs, an additional reactive current is required to enhance the PCC voltage. The amount of the injected reactive current depends on the percentage of the voltage dips as described in (1). For three-phase fault with a fault duration of 150 ms and if the voltage dips are more than 0.6 p.u, the required reactive current should not be less than 1 p.u. However, for voltage dips between 0.1 and 0.6 p.u the injected reactive current should be follow the particular rate where the required reactive current depends on the gain factor k [35]. According to the Egyptian network code, the factor k shall be set between 0 and 4, with 2 being the preferred value [31]. As declared from Fig.4, the FRT is activated as long as the voltage beyond the dead band (V = [0.9 p.u to 1.1 p.u]), i.e. the shaded area.

$$\frac{\Delta I_q}{I_n} = \begin{cases} 1, & \frac{\Delta V}{V_n} < -0.6 \\ k\left(\frac{\Delta V + 0.1}{V_n}\right), & -0.6 \le \frac{\Delta V}{V_n} \\ & \le -0.1, \mathrm{k} \ge 2 \end{cases} \quad (1)$$

where, $\Delta I_q = I_q - I_{q0}$ and $\Delta V = V - V_0$

I_n : The nominal current.
I_q : The reactive current component (quadrature axis component).
I_{q0} : The prefault reactive component.
V_n : The nominal voltage.
V : The voltage of generator during fault.
V_0 : the prefault voltage

Depending on the aforementioned discussion, the goal of the FRT is to increase the reactive current during voltage dip. When the FRT is applied to the RSC and GSC converters at fault condition, the reactive current injected to the grid from the converters can reach up to 1.0 p.u from the converter rating (0.3 p.u w.r.t the DFIG-WT rated capacity). However, for grid fault with voltage dips between 0.1 and 0.6 p.u, there would be a potential for active current flow through converters, which would aid in the restoration of the dc connection capacitor's nominal value by providing its stored energy to the grid [24], [25].

The reference reactive and active currents during FRT can be determined by:

$$I_{q\_ref} = \left(\frac{\Delta I_q}{I_n}\right) I_n \quad (2)$$

$$I_{d\_ref} = \begin{cases} 0, & \frac{\Delta V}{V_n} < -0.6 \\ \sqrt{I_n^2 - I_{q\_ref}^2}, & -0.6 \le \frac{\Delta V}{V_n} \le -0.1 \end{cases} \quad (3)$$

At normal operation the dc link voltage is controlled via GSC. By this way dc link capacitor can be release/ absorbed the active current through GSC to/from grid. Once the fault is detected, GSC follow the FRT requirements (i.e., give the full priority to the reactive current instead of active current) by this means dc link voltage control loop is disabled. As a result, the energy is trapped in the dc link capacitor resulting in a sharp rise of dc link voltage. To protect the dc link capacitor from damage, an alternative protection scheme based on dc chopper is used to keep the dc link voltage with nominal value as shown in Fig.2. This protection scheme is a conventional dc chopper circuit presented in [36]. Based on this scheme resistor is connected in parallel with dc link capacitor by IGBT. The IGBT is triggered through OR logic gate by using two paths as depicted in Fig.2. The first path activates IGBT, if the fault is detected however for the second path, IGBT is triggered if dc link voltage (Vdc) exceeds threshold value (Vdc threshold = 1.1 Vdc)[24], [25], [36].

IV. SYSTEM STABILITY

Maintaining the continuity of the power flow necessitates keeping the wind farm operational rather than tripping when faults occur. As a result, analyzing WT generators for proper stability investigation has become essential.

A. CONCEPT OF IG STABILITY

To explain the concept of IG stability, the torque – speed characteristic of IG is illustrated Fig. 5. The difference between the two modes described in Fig. 5 depends on the generator rotor speed, ω_r. If ω_r is above the grid angular frequency, then the machine works in generator mode otherwise the machine operates in motor mode. As shown in Fig. 5, there are two equilibrium points between T_m and T_e, point "A," and "E." With respect to point "A," the generator works normally with stable operation where $\omega_r = \omega_o$ (ω_o is operating rotor speed)., however point "E" represents unstable point where $\omega_r = \omega_c$ (ω_c is critical rotor speed). When the short circuit fault occurs, the operating point of the generator moves from point "A" to point "B." As a consequence, T_e is suddenly dropped. For the worst case at symmetrical fault, it drops to zero as shown in Fig. (5). Unfortunately, T_m is still exists

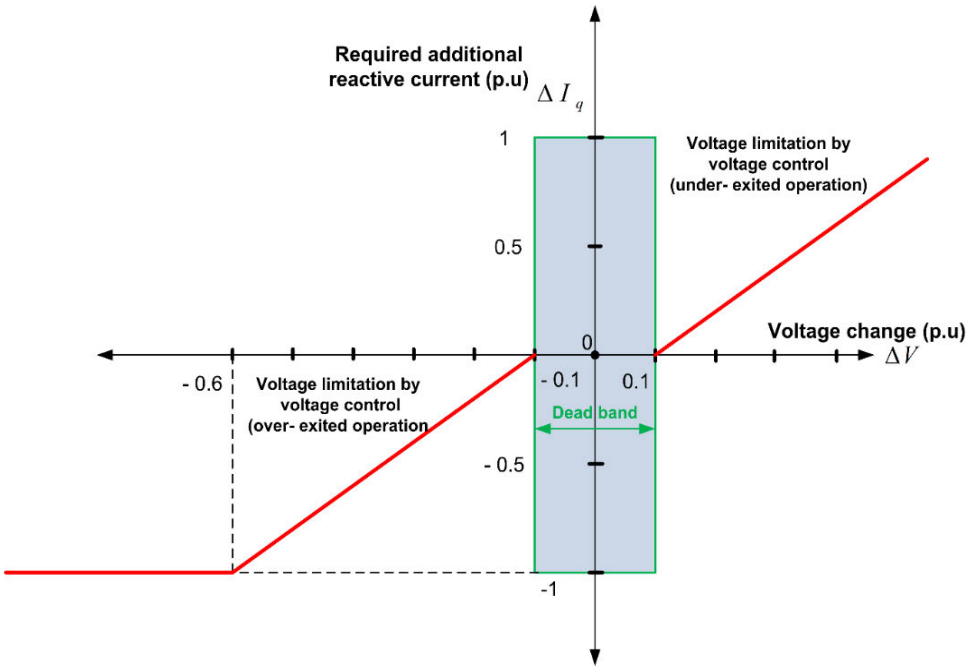

FIGURE 4. Reactive current injection during voltage dips defined by Egyptian grid code.

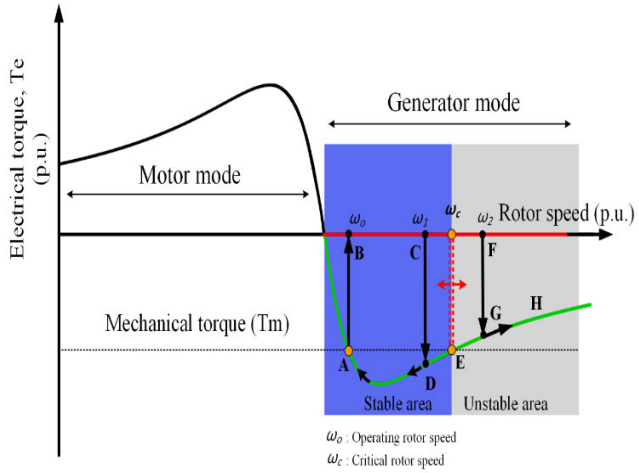

FIGURE 5. Torque – speed characteristic of IG under short circuit faults.

during fault hence, it depends on the incident wind speed. Accordingly the rotor speed of the generator will increase from point "B" (ω_0) towards point "C" (ω_1). Based on the clearance time of the fault, and if the rotor speed is below the critical rotor speed ω_c (i.e generator stability limit), then the operating point moves through path ABCDA, stable area (blue area) where the resultant torque ($T_e - T_m$) enforces the rotor speed to return to its rated point. Otherwise, the operating point moves through path ABCFGH, unstable area (grey area), accordingly the rotor speed increases to not permissible values. In this instant, the protection system disconnects the generator to protect it from damage.

B. PARAMETRIC ANALYSIS OF LYAPUNOV-BASED STABILITY OF SCIG

1) MODELING OFSCIG

In this subsection, the dynamic equations of the IG in terms of d–q components of stator and rotor voltages can be described as [37], [39]:

$$\begin{cases} V_{ds} = R_s I_{ds} + \dfrac{d\lambda_{ds}}{dt} - \omega_s \lambda_{qs} \\ V_{qs} = R_s I_{qs} + \dfrac{d\lambda_{qs}}{dt} + \omega_s \lambda_{ds} \\ V_{dr} = R_r I_{dr} + \dfrac{d\lambda_{dr}}{dt} - (\omega_s - p\omega_r)\lambda_{qr} \\ V_{qr} = R_r I_{qr} + \dfrac{d\lambda_{qr}}{dt} + (\omega_s - p\omega_r)\lambda_{dr} \end{cases} \tag{4}$$

Depending on (4) the rotor and stator quantities can be expressed as subscripts r and s respectively. R_s, R_r are winding resistances, ω_s is the grid angular speed, V is the voltage, and I is the current. Flux linkage (λ) of the stator and the rotor can be expressed as:

$$\begin{cases} \lambda_{ds} = L_s I_{ds} + L_m I_{dr} \\ \lambda_{qs} = L_s I_{qs} + L_m I_{qr} \\ \lambda_{dr} = L_r I_{dr} + L_m I_{ds} \\ \lambda_{qr} = L_r I_{qr} + L_m I_{qs} \end{cases} \tag{5}$$

where, L_s is the stator self- inductance, L_r is the rotor self-inductance while L_m is the mutual inductance.

For SCIG, the rotor voltage V_{dqr}, in the above equations are set zero. The mechanical equation of the SCIG, can be described as:

$$T_m - T_e = J\frac{d\omega}{dt} \tag{6}$$

$$T_m = f\omega_{r0} + T_{m0} \tag{7}$$

where T_m is the total mechanical input of the generator; f represents the viscous friction, J represents rotor moment of inertia, and T_{m0} is the exerted torque to the rotor and by substituting the T_e, the equation (6) can be expressed as:

$$(f\omega_{r0} + T_{m0}) - pL_m\left(I_{qs0}I_{dr0} - I_{ds0}I_{qr0}\right) = J\frac{d\omega}{dt} \tag{8}$$

Depending on (4) - (8), the state space model of SCIG can be described in the form of matrix as [37], [38]:

$$x^{\cdot} = f(x) + B(u) \tag{9}$$

where X, V, f, B, and σ, as shown at the bottom of the page.

Equilibrium conditions of the system are obtained when the system runs with zero deviation state [18]. Accordingly, the equilibrium conditions of SCIG are achieved by putting the derivatives of the dynamic equations of SCIG to zero and substituting SCIG's state variables (i.e., voltages, currents, speed) by its pre-fault values. Consequently, the equilibrium conditions are obtained as:

$$\begin{aligned}
&R_sI_{ds0} - \omega_sL_sI_{qs0} - \omega_sL_mI_{qr0} = V_{ds0}\\
&R_sI_{qs0} - \omega_sL_sI_{ds0} - \omega_sL_mI_{dr0} = V_{qs0}\\
&R_sI_{dr0} - \omega_sL_rI_{qr0} + p\omega_{r0}L_rI_{qr0} - \omega_sL_mI_{qs0}\\
&+p\omega_{r0}L_mI_{qs0} = 0\\
&R_sI_{qr0} - \omega_sL_rI_{dr0} + p\omega_{r0}L_rI_{dr0} - \omega_sL_mI_{ds0}\\
&+p\omega_{r0}L_mI_{ds0} = 0\\
&(-f\omega_{r0} + T_{m0}) - pL_m\left(I_{qs0}I_{dr0} - I_{ds0}I_{qr0}\right) = 0
\end{aligned} \tag{10}$$

To facilitate the Lyapunov analysis of the SCIG, the origin of the system (9) is referred to an equilibrium point given by

$$X_0 \triangleq \begin{bmatrix}\omega_{r0} & I_{ds0} & I_{qs0} & I_{dr0} & I_{qr0}\end{bmatrix}^T$$

which is a solution to (10). The SCIG's state variables around this equilibrium point (X_0), can be described as set of error state variables (e) as:

$$\begin{aligned}
e_1 &\triangleq \omega_r - \omega_{r0}\\
e_2 &\triangleq I_{ds} - I_{ds0}\\
e_3 &\triangleq I_{qs} - I_{qs0}\\
e_4 &\triangleq I_{dr} - I_{qr0}\\
e_5 &\triangleq I_{qr} - I_{qr0}
\end{aligned} \tag{11}$$

The error model of the SCIG about the equilibrium condition can be expressed in terms of a set of error variables (e) by removing the state variables in model (9) and using the error variables given by (11):

$$\frac{d(e)}{dt} = A(x_0)\,e + g(e) \tag{12}$$

where e, $g(e)$, and $A(x_0)$, as shown at the bottom of the next page

2) SYSTEMATIC OF LYAPUNOV BASED STABILITY ANALYSIS

The Lyapunov concept is concerned with the stability of any system as a function of its energy, the EF, which cannot be negative and is described as follows [14]:

$$v = f(x, t) \tag{13}$$

$$v \geq 0 \tag{14}$$

where v is defined as the system energy. The variable x and t are the state variables and time, respectively. If the system disturbed, the system state variables may be changed resulting in change in system energy. If the derivative of the EF w.r.t. time is positive, then the system may be unstable and vice versa [14], [37].

The Lyapunov stability technique is proposed to the SCIG only due to its weak behavior that affect the whole system stability accordingly the EF is determined for the SCIG. The SCIG's Lyapunov EF is derived depending on the energy balance equation which characterizes the energy transfer

$$X \triangleq \begin{bmatrix}\omega_r & I_{ds} & I_{qs} & I_{dr} & I_{qr}\end{bmatrix}^T$$

$$V \triangleq \begin{bmatrix}V_{ds} & V_{qs} & T_{m0}\end{bmatrix}$$

$$f \triangleq (x)\begin{bmatrix}
\frac{pL_m}{J}\left(I_{qs}I_{dr} - I_{ds}I_{qr}\right) - \frac{f}{J}\omega_r\\
\frac{R_r(1-\sigma)}{\sigma L_m}I_{dr} + \frac{pL_m}{\sigma L_s}\omega_rI_{qr} - \frac{R_s}{\sigma L_s}I_{ds} + \frac{p(1-\sigma)}{\sigma}\omega_rI_{qs} + \omega_sI_{qs}\\
\frac{R_r(1-\sigma)}{\sigma L_m}I_{qr} - \frac{pL_m}{\sigma L_s}\omega_rI_{dr} - \frac{R_s}{\sigma L_s}I_{qs} - \frac{p(1-\sigma)}{\sigma}\omega_rI_{ds} - \omega_sI_{ds}\\
\frac{R_s(1-\sigma)}{\sigma L_m}I_{sd} - \frac{pL_m}{\sigma L_r}\omega_rI_{qs} - \frac{R_r}{\sigma L_r}I_{dr} - \frac{p}{\sigma}\omega_rI_{qr} + \omega_sI_{qr}\\
\frac{R_s(1-\sigma)}{\sigma L_m}I_{sq} + \frac{pL_m}{\sigma L_r}\omega_rI_{ds} - \frac{R_r}{\sigma L_r}I_{qr} + \frac{p}{\sigma}\omega_rI_{dr} - \omega_sI_{dr}
\end{bmatrix}$$

$$B \triangleq \begin{bmatrix}
0 & 0 & -\frac{1}{J}\\
\frac{1}{\sigma L_s} & 0 & 0\\
0 & \frac{1}{\sigma L_s} & 0\\
\frac{\sigma-1}{\sigma L_m} & 0 & 0\\
0 & \frac{\sigma-1}{\sigma L_m} & 0
\end{bmatrix}$$

$$\sigma \triangleq 1 - \frac{L_m^2}{L_sL_r}$$

between the input and output of the SCIG based on the principle of energy conservation [14], [18]. Consequently, the energy balance equation can be expressed in terms of SCIG mechanical and magnetic field energies, W_J and W_f, which can be defined as [38], [39].

$$W_f = \frac{1}{2}\mathrm{L_s}\left(\mathrm{I_{ds}^2}+\mathrm{I_{qs}^2}\right)+\frac{1}{2}\mathrm{L_r}\left(\mathrm{I_{dr}^2}+\mathrm{I_{qr}^2}\right) +\mathrm{L_m}\begin{bmatrix}\mathrm{I_{ds}} & \mathrm{I_{qs}}\end{bmatrix}\begin{bmatrix}\mathrm{I_{dr}}\\ \mathrm{I_{qr}}\end{bmatrix} \tag{15}$$

$$W_J = \frac{1}{2}\mathrm{J}\omega_{\mathrm{r}}^2 \tag{16}$$

To facilitate the Lyapunov concept, W_f and W_J can be expressed in terms of a set of error state variables (e) about the equilibrium points that correspond to the pre-fault values of the SCIG's state variables.

Depending on the set of error state variables in (11), Eqs. (15) and (16) can be changed as:

$$\begin{aligned}W_f &= \frac{1}{2}L_s\left(e_2^2+e_3^2+2e_2I_{ds0}+2e_3I_{qs0}\right)\\ &+\frac{1}{2}L_r\left(e_4^2+e_5^2+2e_4I_{dr0}+2e_5I_{qr0}+L_me_2e_4\right)\\ &+L_m\left(I_{ds0}e_4+e_2I_{dr0}+e_3e_5+I_{qs0}e_5+e_3I_{qr0}\right)\\ &+\frac{1}{2}L_s\left(I_{ds0}^2+I_{qs0}^2\right)+\frac{1}{2}L_r\left(I_{dr0}^2+I_{qr0}^2\right)\\ &+L_m(I_{ds0}I_{dr0}+I_{sq0}I_{qr0})\end{aligned} \tag{17}$$

$$W_J = \frac{1}{2}J\left(e_1^2+2e_1\omega_{r0}\right)+\frac{1}{2}J\omega_{r0}^2 \tag{18}$$

Now the energy balance equation $W(e)$ can be defined by

$$W(e) = W_f + W_J - W_f(0) - W_J(0) \tag{19}$$

$W_f(0)$ and $W_J(0)$ are the initial magnetic and mechanical energies, respectively. These energies represent the equilibrium condition based on the set-points of the state space variables of the SCIG (currents and speed) which represented by the pre-fault values $\mathrm{I_{ds0}}$, $\mathrm{I_{qs0}}$, $\mathrm{I_{dr0}}$, $\mathrm{I_{qr0}}$ and ω_{r0} as shown below:

$$\begin{aligned}W_f(0) &= \frac{1}{2}\mathrm{L_s}\left(\mathrm{I_{ds0}^2}+\mathrm{I_{qs0}^2}\right)+\frac{1}{2}\mathrm{L_r}\left(\mathrm{I_{dr0}^2}+\mathrm{I_{qr0}^2}\right)\\ &+\mathrm{L_m}(\mathrm{I_{ds0}I_{dr0}}+\mathrm{I_{qs0}I_{qr0}})\end{aligned} \tag{20}$$

$$W_J(0) = \frac{1}{2}\mathrm{J}\omega_{\mathrm{r0}}^2 \tag{21}$$

Then,

$$\begin{aligned}W(e) &= \begin{bmatrix}e_1\\ e_2\\ e_3\\ e_4\\ e_4\end{bmatrix}\begin{bmatrix}\frac{J}{2} & 0 & 0 & 0 & 0\\ 0 & \frac{L_s}{2} & 0 & \frac{L_m}{2} & 0\\ 0 & 0 & \frac{L_s}{2} & 0 & \frac{L_m}{2}\\ 0 & \frac{L_m}{2} & 0 & \frac{L_r}{2} & 0\\ 0 & 0 & \frac{L_m}{2} & 0 & \frac{L_r}{2}\end{bmatrix}\\ &[e_1\ e_2\ e_3\ e_4\ e_5]\\ &+\left[J\omega_{r0}\ L_sI_{ds0}+L_mI_{dr0}\ L_sI_{qs0}\right.\\ &\left.+L_mI_{qr0}\ L_rI_{dr0}+L_mI_{ds0}\ L_rI_{qr0}+L_mI_{qs0}\right]\\ &[e_1e_2e_3e_4e_5]\end{aligned} \tag{22}$$

Accordingly, $W(e)$ can be rewritten in matrix format as:

$$W(e) = e^TPe + d^Te \tag{23}$$

where

$$P = \frac{1}{2}\begin{bmatrix}J & 0 & 0 & 0 & 0\\ 0 & L_s & 0 & L_m & 0\\ 0 & 0 & L_s & 0 & L_m\\ 0 & L_m & 0 & L_r & 0\\ 0 & 0 & L_m & 0 & L_r\end{bmatrix}$$

$$d = \begin{bmatrix}J\omega_{r0}\\ L_sI_{ds0}+L_mI_{dr0}\\ L_sI_{qs0}+L_mI_{qr0}\\ L_rI_{dr0}+L_mI_{ds0}\\ L_rI_{qr0}+L_mI_{qs0}\end{bmatrix}$$

$$e = [e_1e_2e_3e_4e_5]^T$$

$$g(e) = \begin{bmatrix}\frac{pL_m}{J}e_3e_4-\frac{pL_m}{J}e_2e_5\\ \frac{pL_m}{\sigma L_s}e_1e_5+\frac{p(1-\sigma)}{\sigma}e_1e_3\\ -\frac{pL_m}{\sigma L_s}e_1e_4-\frac{p(1-\sigma)}{\sigma}e_1e_2\\ -\frac{pL_m}{\sigma L_r}e_1e_3-\frac{p}{\sigma}e_1e_4\\ \frac{pL_m}{\sigma L_r}e_1e_3+\frac{p}{\sigma}e_1e_4\end{bmatrix}$$

$$A(x_0) = \begin{bmatrix}\frac{f}{J} & -\frac{pL_m}{J}i_{qr0} & \frac{pL_m}{J}i_{dr0} & \frac{pL_m}{J}i_{qs0} & -\frac{pL_m}{J}i_{ds0}\\ \frac{p(1-\sigma)}{\sigma}\left(\frac{L_r}{L_m}I_{qr0}+I_{qs0}\right) & -\frac{R_s}{\sigma L_s} & \frac{p(1-\sigma)}{\sigma}\omega_{r0}+\omega_s & \frac{R_r(1-\sigma)}{\sigma L_m} & \frac{pL_m}{\sigma L_s}\omega_{r0}\\ -\frac{p(1-\sigma)}{\sigma}\left(\frac{L_r}{L_m}I_{dr0}+I_{ds0}\right) & -\frac{p(1-\sigma)}{\sigma}\omega_{r0}-\omega_s & -\frac{R_s}{\sigma L_s} & -\frac{pL_m}{\sigma L_s}\omega_{r0} & \frac{R_r(1-\sigma)}{\sigma L_m}\\ -\frac{p}{\sigma}\left(\frac{L_m}{L_r}I_{qs0}+I_{qr0}\right) & \frac{R_s(1-\sigma)}{\sigma L_m} & -\frac{pL_m}{\sigma L_r}\omega_{r0} & -\frac{R_r}{\sigma L_r} & -\frac{p}{\sigma}\omega_{r0}+\omega_s\\ \frac{p}{\sigma}\left(\frac{L_m}{L_r}I_{ds0}+I_{dr0}\right) & \frac{pL_m}{\sigma L_r}\omega_{r0} & \frac{R_s(1-\sigma)}{\sigma L_m} & \frac{p}{\sigma}\omega_{r0}-\omega_s & -\frac{R_r}{\sigma L_r}\end{bmatrix}$$

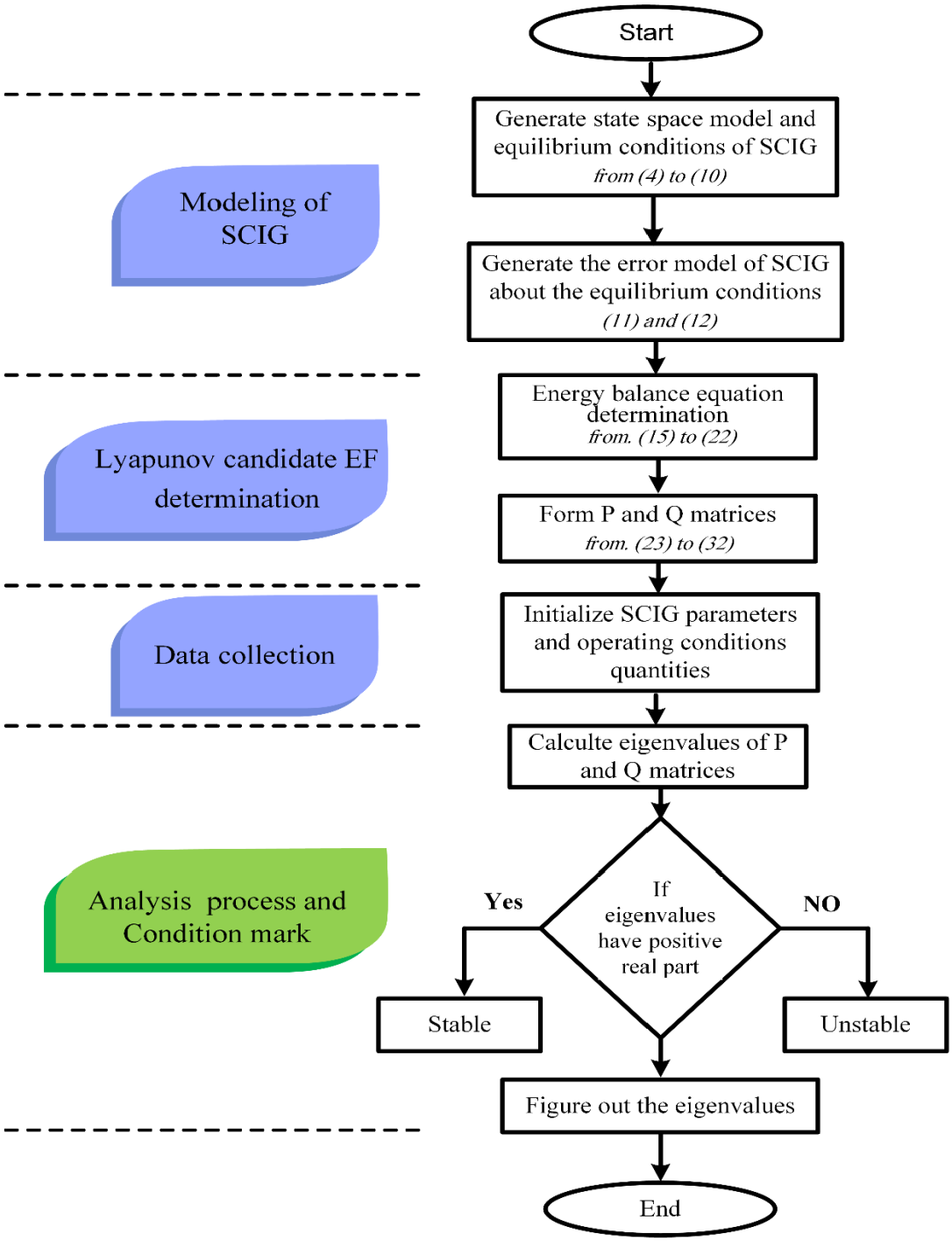

FIGURE 6. The flowchart of the proposed Lyapunov method.

The power balance equation of SCIG is the derivative of the EF, which can be deduced in terms of generator quantities as [37], [38]:

$$\frac{dW(e)}{dt} = \begin{bmatrix} V_{ds} & V_{qs} & T_m \end{bmatrix} \begin{bmatrix} -I_{ds} \\ -I_{qs} \\ \omega_r \end{bmatrix} - R_s I_{ds}^2 - R_s I_{qs}^2 - R_r I_{dr}^2 - R_r I_{qr}^2 \quad (24)$$

Using (11), rewrite Eq. (24) in terms of error variables taken into account the equilibrium conditions

$$\frac{dW(e)}{dt} = \left(f e_1^2 + 2f\omega_{r0} e_1 + T_{m0} e_1\right) - (V_{ds} e_2 + V_{qs} e_3) - R_s\left(e_2^2 + 2e_2 I_{ds0}\right) - R_s\left(e_3^2 + 2e_3 I_{qs0}\right) - R_r\left(e_4^2 + 2e_4 I_{dr0}\right) - R_r\left(e_5^2 + 2e_5 I_{qr0}\right) \quad (25)$$

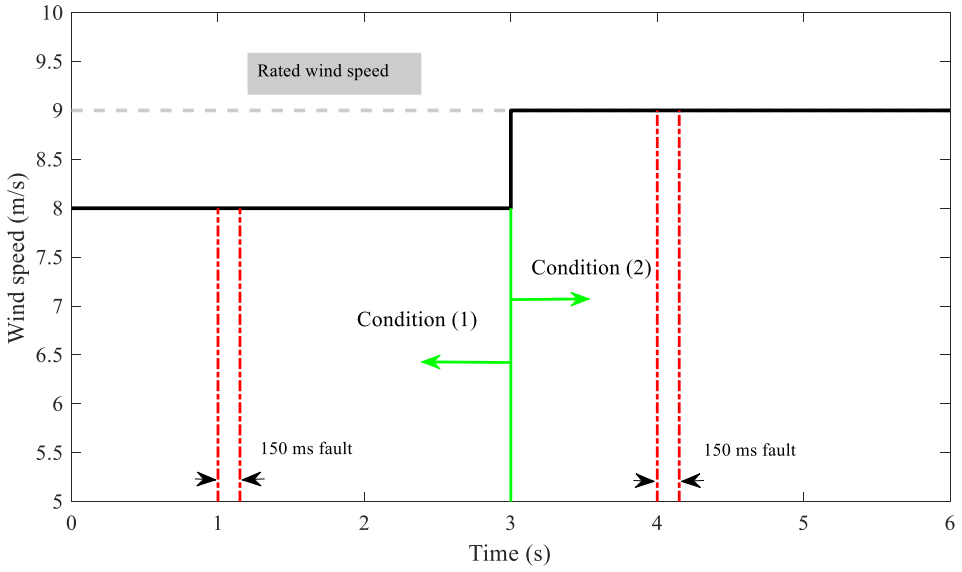

FIGURE 7. Wind speed profile with fault cases.

Which can be rewritten as:

$$\frac{dW(e)}{dt} = -\begin{bmatrix} e_1 \\ e_2 \\ e_3 \\ e_4 \\ e_4 \end{bmatrix} \begin{bmatrix} f & 0 & 0 & 0 & 0 \\ 0 & R_s & 0 & 0 & 0 \\ 0 & 0 & R_s & 0 & 0 \\ 0 & 0 & 0 & R_r & 0 \\ 0 & 0 & 0 & 0 & R_r \end{bmatrix} [e_1 e_2 e_3 e_4 e_5] - \left[-2f\omega_{r0} - T_{m0}\omega_{r0} \;\; 2R_s I_{ds0} + V_{ds0} \;\; 2R_s I_{qs0} + V_{ds0} 2R_r I_{dr0} \;\; 2R_r I_{qr0}\right] [e_1 e_2 e_3 e_4 e_5]$$

Putting $\frac{dW(e)}{dt}$ in the form of matrix, shown below,

$$\frac{dW(e)}{dt} = -e^T Q_W e - c_W^T e \tag{26}$$

where

$$Q_W = \begin{bmatrix} f & 0 & 0 & 0 & 0 \\ 0 & R_s & 0 & 0 & 0 \\ 0 & 0 & R_s & 0 & 0 \\ 0 & 0 & 0 & R_r & 0 \\ 0 & 0 & 0 & 0 & R_r \end{bmatrix}$$

$$c_W = \begin{bmatrix} -2f\omega_{r0} - T_{m0} \\ 2R_s I_{ds0} + V_{ds0} \\ 2R_s I_{qs0} + V_{ds0} \\ 2R_r I_{dr0} \\ 2R_r I_{qr0} \end{bmatrix}$$

From (23), the derivative of the energy balance $W(e)$ can be described as:

$$\frac{dW(e)}{dt} = e^T P \frac{d(e)}{dt} + \frac{d(e^T)}{dt} Pe + d^T \frac{d(e)}{dt} \tag{27}$$

From (26),

$$e^T P \frac{d(e)}{dt} + \frac{d(e^T)}{dt} Pe + d^T \frac{d(e)}{dt} = -e^T Q_W e - c_W^T e \tag{28}$$

Consequently,

$$e^T P \frac{d(e)}{dt} + \frac{d(e^T)}{dt} Pe = -e^T Q_W e - c_W^T e - d^T \frac{d(e)}{dt} \tag{29}$$

The candidate Lyapunov EF is [38,40]:

$$V(e) \equiv e^T Pe$$

Thus,

$$\frac{dV(e)}{dt} \equiv e^T P \frac{d(e)}{dt} + \frac{d(e^T)}{dt} Pe = -e^T Q_W e - c_W^T e - d^T \frac{d(e)}{dt} \tag{30}$$

From (12), $\frac{d(e)}{dt} = A(x_0)\, e + g(e)$

So

$$\frac{dV(e)}{dt} = -e^T Q_W e - c_W^T e - d^T (A(x_0)\, e + g(e)) \tag{31}$$

Taken,

$$\mathrm{e^T Qe} = e^T Q_W e + d^T g(e)$$
$$\mathrm{c^T e} = c_W^T e + d^T A(x_0)\, e$$

Which can be rewritten as:

$$\frac{\mathrm{dV}}{\mathrm{dt}} = -\mathrm{e^T Qe} - \mathrm{c^T e} \tag{32}$$

where C and Q, as shown at the bottom of page 12.

According to (10), components of C represent the equilibrium conditions and therefore C ≡ 0

Consequently, the Lyapunov function (LF) and its derivative w.r.t. time are:

$$\begin{cases} v(e) = e^T Pe \\ \dfrac{dv}{dt} = -e^T Qe \end{cases} \tag{33}$$

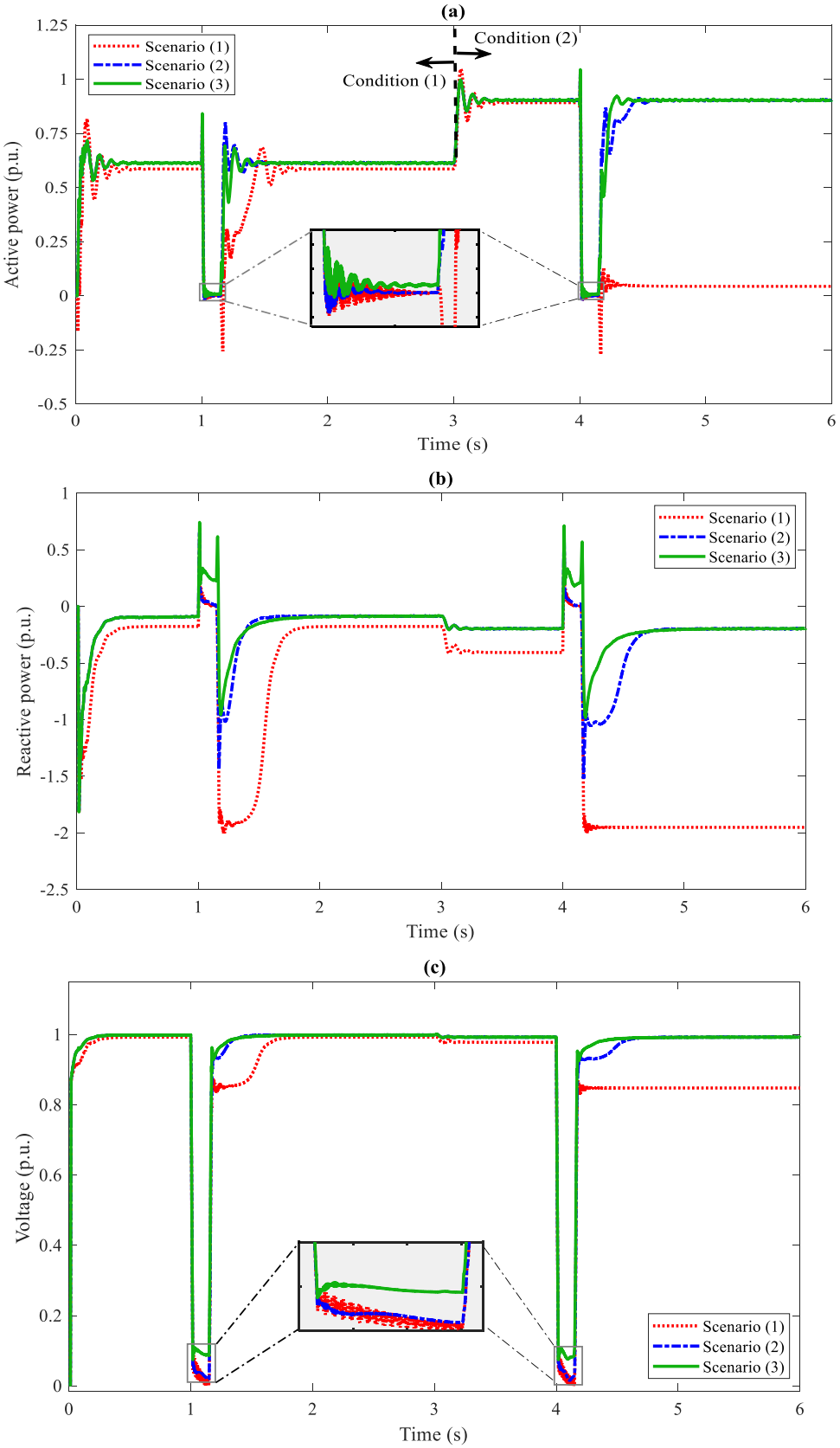

FIGURE 8. Simulation reuslts of the three scenatios under the two operating conditions.

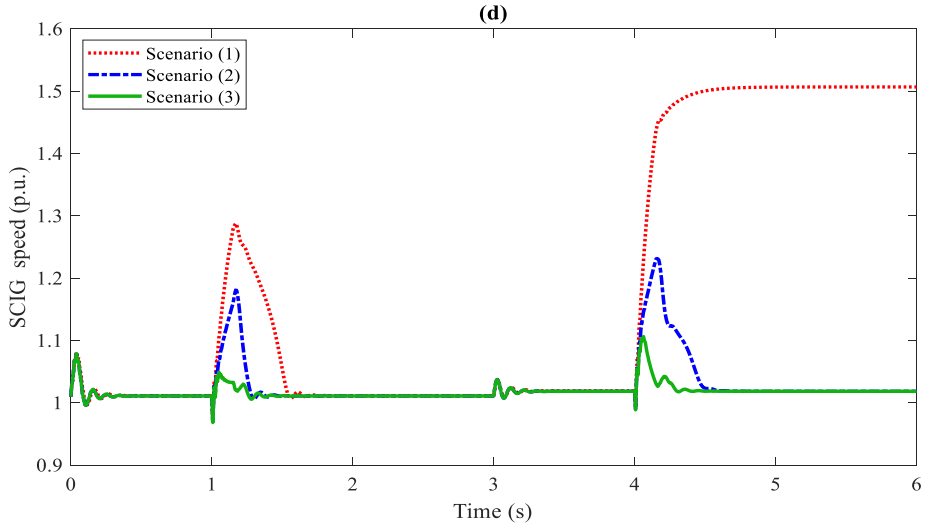

FIGURE 8. *(Continued.)* **Simulation reuslts of the three scenatios under the two operating conditions.**

Based on the Lyapunov theory, If the following constrains (i.e. LF and its derivative) are achieved, the stability of the SCIG is realized [14], [37], [40]:

(a)

$$v(e) > 0 \quad \forall e \neq 0, \text{ and } v(e) = 0 \tag{34}$$

(b)

$$\frac{dv}{dt} < 0 \quad \forall e \neq 0.$$

from (34), to achieve the contains (a) and (b), accordingly realize the stability of SCIG, the matrices P and Q should be positive definite. Alternatively, P and Q are positive definite if all of their eigenvalues have a positive real part [14]. Consequently, in order to determine the stability of SCIG, eigenvalues of the P and Q should be monitored. The flow chart of the proposed Lyapunov method to analysis conditions for global asymptotic stability of the SCIG is depicted in Fig. (6).

V. RESULTS AND DISCUSSION

The analytical approach of the Lyapunov theory and the proposed FRT scheme are applied to the hybrid wind farm illustrated in Fig.1. The whole configuration of the system along with the hybrid wind farm is simulated with MATLAB/Simulink software. Different case studies are considered. These are:

- Case I: The performance of the proposed hybrid wind farm at fault condition with FRT
- Case II: The simulation and experimental validation of FRT of DFIG- WT
- Case III: The proposed wind farm's stability is assessed using the Lyapunov theory.

A. CASE I

The system stability with the FRT is tested through three scenarios according to the type of wind farms. These are:

Scenario (1): The wind farm consists of only SCIG-WTs with rating capacity 20.400 MW

$$C = \begin{bmatrix} -pL_m\left(I_{qs0}I_{dr0} - I_{ds0}I_{qr0}\right) + f\omega_{r0} + T_{m0} \\ R_sI_{ds0} - \omega_s\left(L_sI_{qs0} + L_mI_{qr0}\right) - U_{ds} \\ R_sI_{qs0} + \omega_s\left(L_sI_{ds0} + L_mI_{dr0}\right) - U_{qs} \\ R_rI_{dr0} - S\omega_s\left(L_rI_{qr0} + L_mI_{qs0}\right) \\ R_rI_{qr0} + S\omega_s\left(L_rI_{dr0} + L_mI_{ds0}\right) \end{bmatrix}$$

$$Q = \begin{bmatrix} f & \frac{1}{2}pL_mI_{qr0} & -\frac{1}{2}pL_mI_{dr0} & \frac{1}{2}pL_rI_{qr0} & -\frac{1}{2}pL_rI_{dr0} \\ \frac{1}{2}pL_mI_{qr0} & R_s & 0 & 0 & -\frac{f}{2}L_mp\omega_{r0} \\ -\frac{1}{2}pL_mI_{dr0} & 0 & R_s & \frac{1}{2}L_mp\omega_{r0} & 0 \\ \frac{f}{2}pL_rI_{qr0} & 0 & \frac{1}{2}L_mp\omega_{r0} & R_r & 0 \\ -\frac{1}{2}pL_rI_{dr0} & -\frac{1}{2}L_mp\omega_{r0} & 0 & 0 & R_r \end{bmatrix}$$

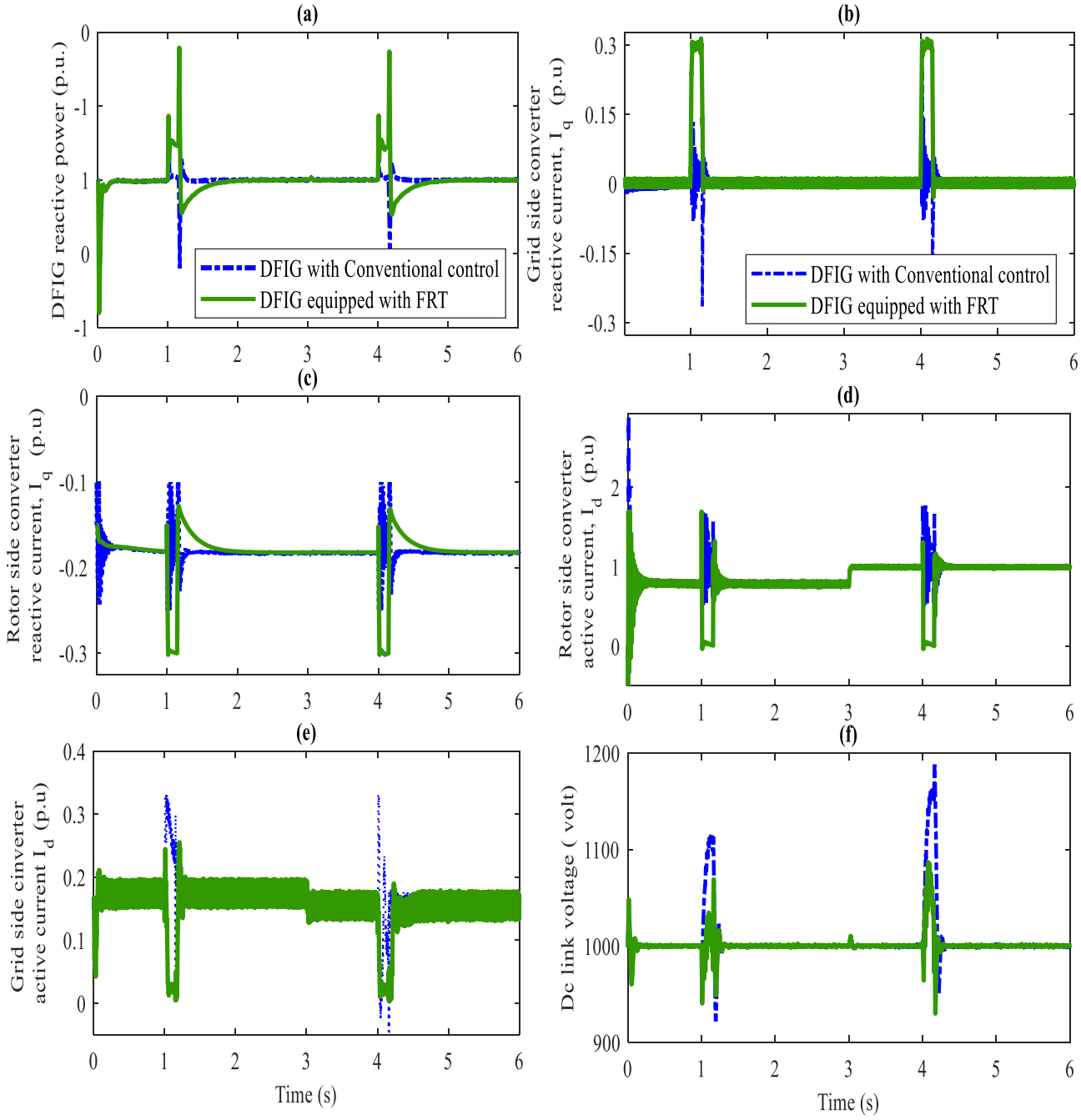

FIGURE 9. Simulation reuslts of the response of DFIG with and without proposed FRT.

$(2\times(17\times600))$ kW. This is two tranches from 'Danish' wind farm in Zafarana.

Scenario (2): The wind farm with rating capacity 20.400 MW with (17 × 600 kW) SCIG-WTs and (12 × 850 kW) DFIGs-WTs as conducted in Fig.1.

Scenario (3): The wind farm composed of the same numbers of SCIG and DFIG as in scenario (2) but the DFIGs are equipped with the FRT.

The three scenarios are examined under two different operating conditions. In the first condition, the wind farm is subjected to fault incident at the instant 1 s and cleared after 150 ms, where the wind speed value is below the rated wind speed. While in the second condition, the wind farm is subjected to the same fault condition as the first condition, but the fault occurred at t = 4 s, wind farm operates at rated wind speed. To evaluate the performance of FRT under the worst grid fault conditions, a three-phase to ground fault is

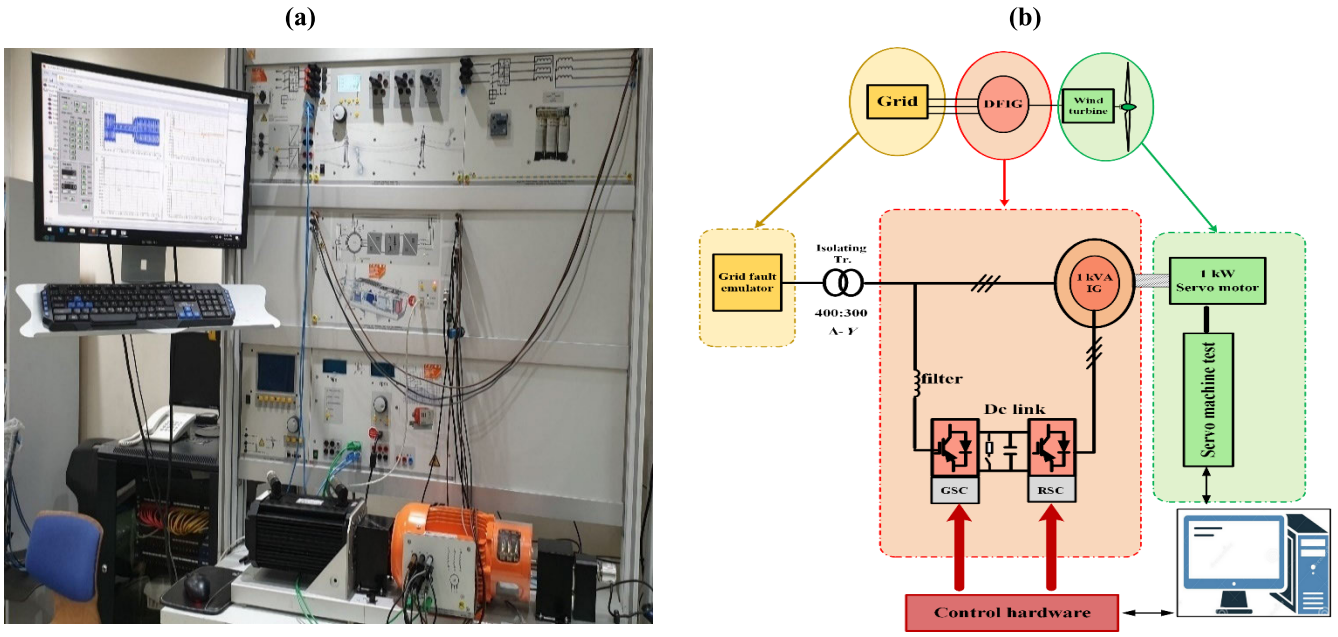

FIGURE 10. Expermintal setup of a DFIG system (a) Schematic diagram. (b) Platform diagram.

occurred at the nearest bus to the DFIG terminals as shown in Fig.1. Fig. 7 shows the portrayed wind speed profile with the two operating conditions.

Fig. 8 describes the dynamic performance of the three scenarios under the two conditions described before.

As shown in Fig.8(a) and before initiating the fault (condition (1)), SCIG based wind farm produces less injected active power therefore it has not the ability to track the MPP. It also absorbs large reactive power, Fig.8(b), which means that it has not the ability for reactive power control compared with other scenarios. The PCC voltage and SCIG speed are the same for the three scenarios, where they operate at steady state. However, scenario (1) has slightly lower voltage due to large absorbed reactive power as shown in Fig. 8(b) and (c), respectively. Once the fault initiated at t = 1 s, the voltage at PCC and the injected active power is dropped as shown in Fig. 8(c) and (a), respectively. As consequence the SCIG speed increased, Fig.8(d), where the equilibrium condition between the mechanical and electrical powers of the generator is not maintained. As shown in Fig.8(b), a significant amount of reactive power is consumed to re-establish the magnetic field as the generator speed increases after the fault is cleared resulting in voltage decrease at the PCC as illustrated in Fig.8(c). The stability of the three scenarios is restored after clearing the fault as depicted from Fig.8(a); however, scenario (3) maintains better stability and recovers faster compared with the other scenarios. The preferable features of scenario (3) are attributed to its capability to reactive power compensation during fault period as shown in Fig.8(b).

It keeps the voltage slightly higher than other scenarios accordingly the injected active power almost represents the same voltage scenario as shown in Fig. 8(c) and (a).

A new operating point is established when the wind speed is increased (condition (2)). The absorbed reactive power of the three scenarios is increased especially in scenario (1) which has no self-compensation. Accordingly, when the fault is occurred at t = 4 s, scenario (1) cannot withstand the same fault conditions as condition (1), where the SCIG speed exceeds the allowed limit as shown in Fig. 8(d). After clearing the fault, the absorbed reactive power is increased significantly, Fig.8(b) leading to voltage collapse at the PCC as conducted in Fig. 8(c). As a result, the system loses its stability in scenario (1), with the injected active power failing to recover to its nominal value, as shown in Fig. 8. (a). Scenarios (2) and (3), on the other hand, are stable and restore pre-fault values, but scenario (3) has a faster recovery response once the fault is cleared, as shown in the green line for all quantities in Fig.8.

B. CASE II

The individual response of the DFIG equipped with FRT or using conventional control is described in Fig.9. With conventional control, the DFIG produces its own reactive power (i.e. work with unity power factor) as shown in Fig.9(a) accordingly the overall absorbed reactive power is reduced. However, for DFIG equipped with FRT, extra reactive power can be produced during the fault, Fig.9(a). This reactive power is necessary for compensating the SCIG reactive power and hence recovery the pre-fault value faster as conducted in Fig.9(b). The reactive power compensation of DFIG equipped with FRT is attributed to reactive current injection of the converters. According to the Egypt grid code, the reactive current injection should reach 100% of converter rating (i.e. 0.3 p.u with respect to the rated capacity of

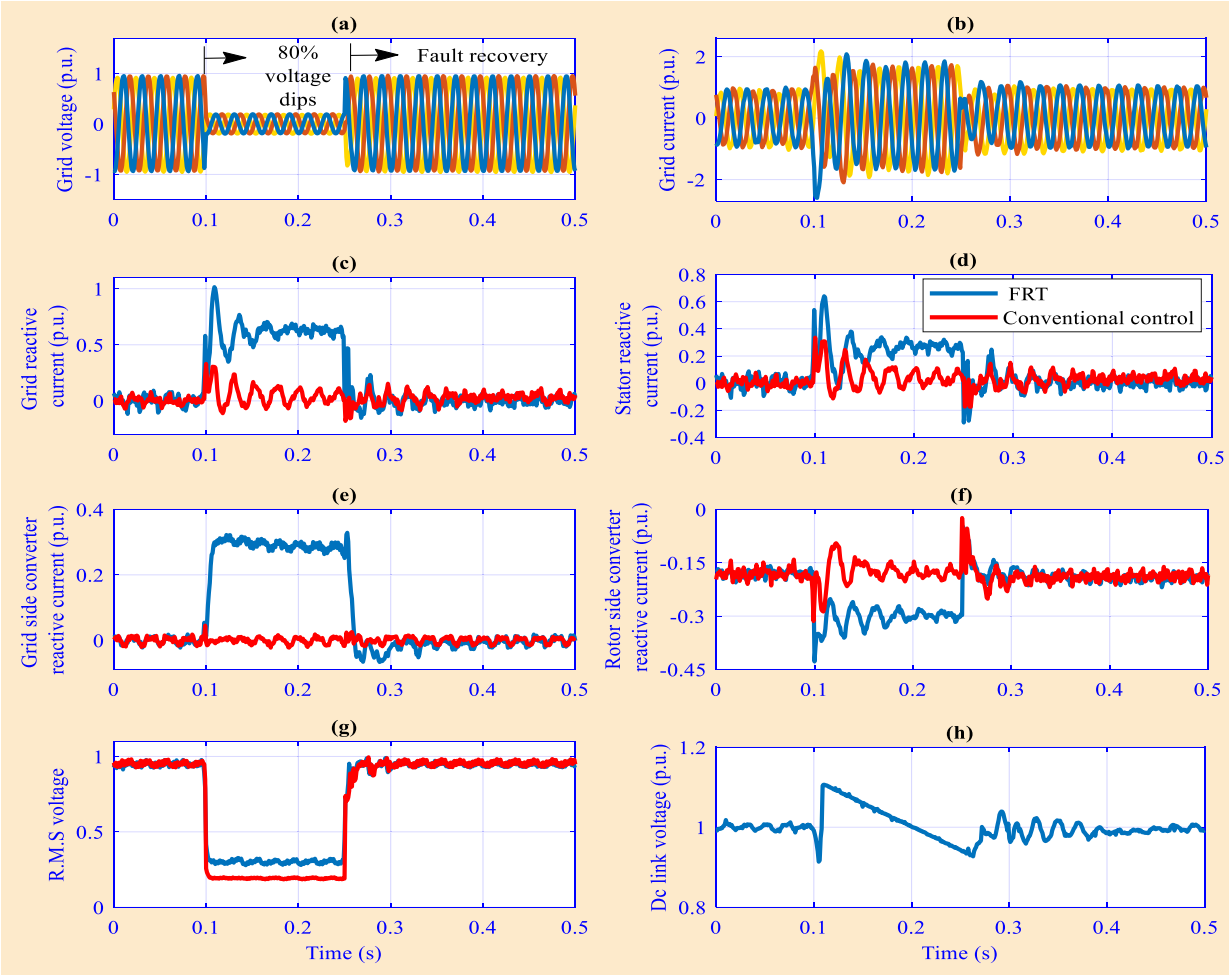

FIGURE 11. Experimental results of the 1 kVA test rig grid connected DFIG with and without FRT to symmetrical three phase fault under 80 % voltage dips.

DFIG-WT) when the voltage dips more than 60% (100% in this case), which is achieved as shown in Figs.9(b) and (c). It is important to point out, at the absence of fault, the RSC produces reactive current for the generator magnetizing condition. However, the GSC supplies no reactive current to ensure working with unity power factor. The DFIG equipped with FRT forces the converters to give the priority of reactive current flow during fault. Consequently, the controller adjusts the active current through the converters by modifying its reference value to follow the grid code requirements. By this means the active current injection should be reduced to zero as conducted in Fig.9(d) and (e). During normal operation, GSC maintains dc-link voltage constant however, under grid fault condition, the FRT is activated and the injected active is intentional dropped.

At this case, the dc link voltage control loop is disabled temporary, and the energy trapped in the dc link cannot be released accordingly a sharp rise to the dc link voltage occurred. As a consequence, the excess energy gives a sharp rise in the dc link voltage, Fig. 9(f) (i.e., normal control). However, with FRT, the dc chopper is used to mitigate the over voltage of dc link voltage as shown in Fig. 9(f). Further, when the voltage dips reach value above the level 0.6 p.u, there will be a flow of active current through converters.

To validate the concept of the FRT of DFIG-WT practically, 1 kVA test rig grid connected DFIG-WT system with the Lab soft environment is used as shown in Fig. 10. The test rig permits the performance evaluation of the DFIG system experimentally to verify the proposed method of reactive power compensation under grid fault conditions. The main elements of the test rig system can be described as following:

1) 1 kW servo-machine test bench for WT simulator. This test bench system provides a torque input to the DFIG. Moreover, provides a simulated mechanical model by its control hardware to create the torque input from a WT rotor.
2) A 1 kVA DFIG system including 0.8 kW, 400/230, 50 Hz three phase IG, two controlled three-phase inverter, integrated brake chopper and integrated power switch for connecting the generator to the grid.
3) A dynamic grid fault simulator to simulate the voltage dip profiles. The dynamic grid fault simulator unit is

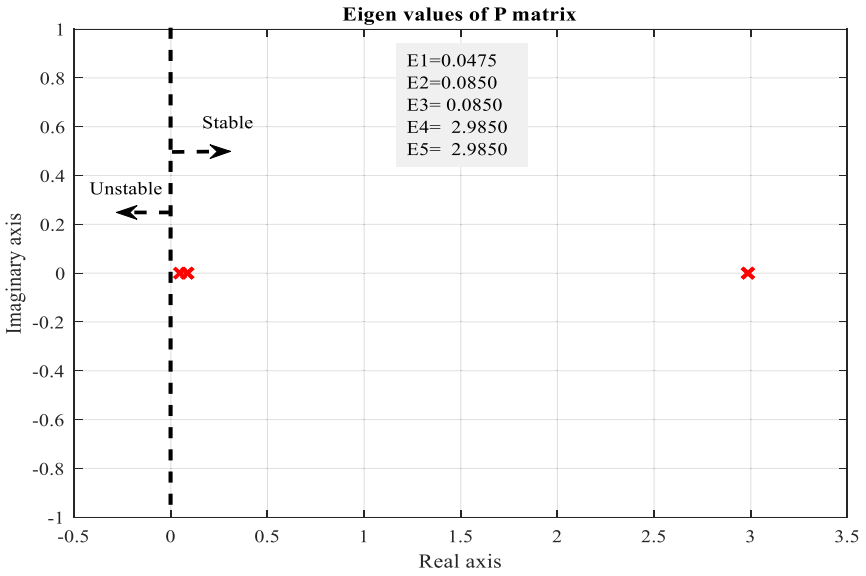

FIGURE 12. Eigenvalues of the P matrix.

connected to the DFIG system via a 400:300 $\Delta - Y$ isolation transformer.

4) A control hardware which contains a combination of digital controller, interface boards, isolated sensing equipment, and a dedicated PC, which all used to execute the DFIG controller, WT simulator and fault test control. The schematic diagram and platform diagram of the experimental setup of a DFIG system are presented in Fig. 10 (a) and (b), respectively.

The test rig DFIG system is examined with 150 ms 3-phase to ground fault with 80% voltage dips to validate the effectiveness of reactive power compensation on the performance of the DFIG. It is worth to mention that, 100% voltage dips are not excited because the converters are disabled by the controller (pulse inhibition) where the phase position is not known as a consequence there is no current fed to the grid. The conducted experimental results have been presented in Fig. 11. The data extracted from the test rig system is drawn using the MATLAB software. The instantaneous values of the grid voltage and injected grid current are shown in Fig. 11 (a) and (b), respectively. As described in Fig.11 (a) the 3-phase to ground fault with 80% voltage dips is initiated at the instant 0.1 s and cleared at 0.25 s.

As a consequence, the current increases as conducted in Fig.11(b). In the absence of fault, the test rig DFIG system supplies no reactive current to the grid, Fig. 11(c), (i.e. work with unity power factor). In this case, the DFIG produces its own reactive power by the injected reactive current from the RSC for the generator magnetizing condition, Fig. 11(f).

However, in the event of fault and with the FRT, the test rig DFIG system supplies reactive current to the grid, Fig.11(c), to compensate the voltage dips as shown from Fig.11(g). The reactive power compensation of the DFIG system is attributed to the reactive current injection of the RSC and GSC.

The grid reactive current, Fig. 11(c), is the sum of the stator reactive current, Fig. 11(d), and the GSC reactive current, Fig. 11(e). According to the grid code, the current injection of the converters should reach 100% of converter rating (i.e. 0.3 pu with respect to the rated capacity of the DFIG-WT. When the voltage dips more than 60% (80% in this case) which achieved as shown in Fig. 11(e) and (f). the injected grid reactive current compensates the voltage to slightly higher values than the DFIG with the conventional control as shown in Fig. 11(g). In the event of fault, a brake chopper as amendatory action protects the dc link, where it has been engaged automatically when the dc link voltage increased above threshold value. The dc link voltage is shown in Fig. 11(h).

C. CASE III

The stability of the SCIG of the proposed wind farm shown in Fig. 1 is investigated in this subsection employing the LF method. To validate the system stability using the Lyapunov-based method, the matrices P and Q have to be determined firstly then their eigenvalues are determined. If their eigenvalues are positive, then the two matrices are positive definite. As a result, the constraints in (34) are met, and the system is stable; otherwise, it is unstable. Matrix P and its eigenvalue is calculated using the system parameters shown in the Appendix A. It is shown from Fig. 12 that all the eigenvalues of matrix P are positive indicating that matrix P is positive definite. However, P does not change w.r.t the system's operating conditions where it depends only on the SCIG parameters. The matrix Q, on the other hand, is dependent on the SCIG's operating condition (e.g., speed and current). This implies that the system stability is determined by the eigenvalues of Q. To calculate the Q, consider the time-domain simulation of the proposed wind farm using

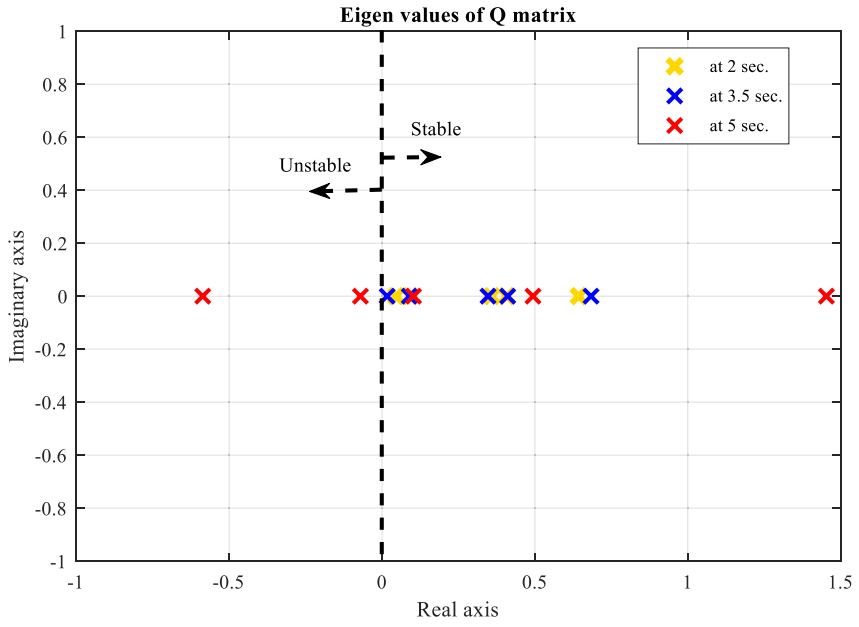

FIGURE 13. Eigenvalues of the Q matrix for scenario (1) at different time interval.

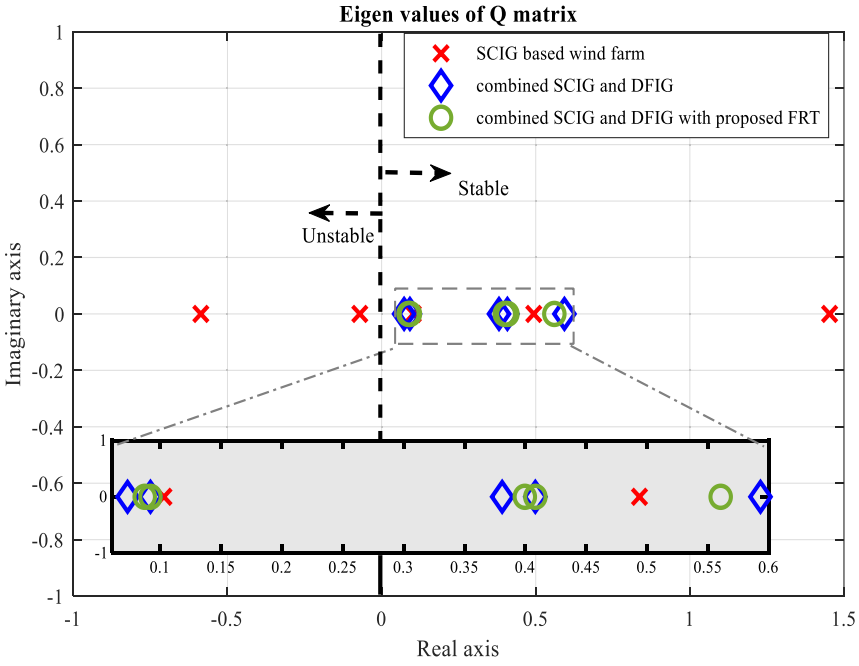

FIGURE 14. Eigenvalues of the Q matrix of the three scenarios at instant 5 s.

the Matlab/Simulink tool. The system is stable if all of Q's eigenvalues are positive. If one eigenvalue has a negative real part then the system is unstable.

The eigenvalues of the Q matrix for scenario (1), mentioned in Case I, at different time intervals (i.e. 2 s, 3.5 s, and 5 s) where SCIG operating conditions that are changed are depicted in Fig.13. For example, at instant 2 s, when the SCIG system recovers its state after the fault (which initiated at 1 s), the Q matrix and its eigenvalue are calculated. They are also determined at 3.5 s after the operation is changed (i.e. wind speed changes). After the SCIG system recovers its state after the fault (which initiated at 4 s), the Q and its eigenvalue are calculated at instant 5 s. As shown in Fig. 13, for instants 2 and 3.5 s, all eigenvalues are positive, indicating stable operation; however, for instant 5 s, two eigenvalues are negative, indicating unstable operation. The eigenvalues of Q for the three scenarios wind farms, mentioned in Case I, at instant 5 s are analyzed in Fig. 14. All eigenvalues in

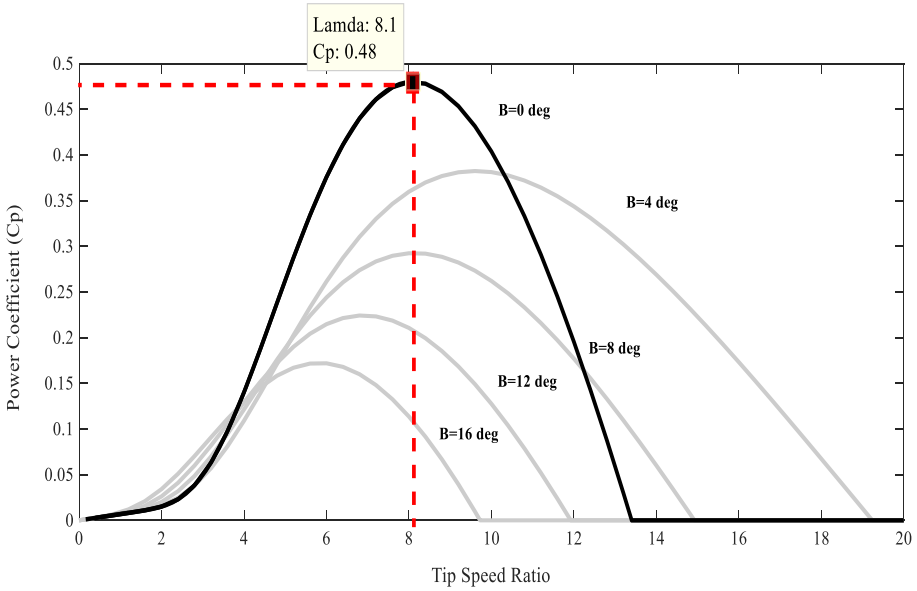

FIGURE 15. Cp – λ curves for various β values.

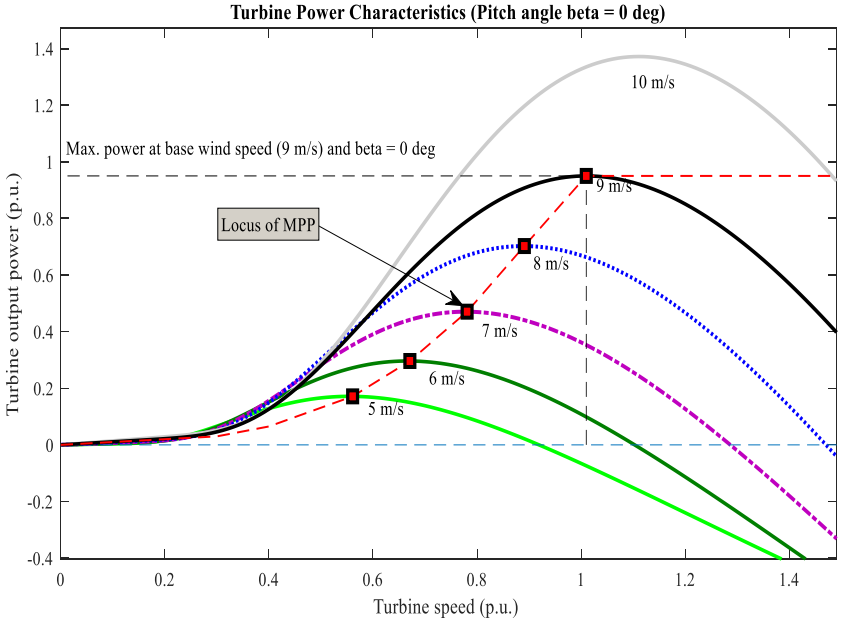

FIGURE 16. Extracted mechanical power with WT rotor speed for various values of wind speed.

scenarios (2) and (3) are positive, indicating a stable operation. However, in scenario (1), two eigenvalues are negative at the same instant resulting in unstable operation of the SCIG. It is remarked that there is a high level of agreement between Lyapunov-based stability assessment's results and the simulation results.

VI. CONCLUSION

This paper has addressed the stability of hybrid wind farms composed of SCIG and DFIG of Zafarana, Suez Gulf area, Egypt. The parameters of FRT curve of Egypt grid code have been utilized. A global stability of the SCIG in the sense of Lyapunov has been identified and tested by time domain simulation. The dynamic behavior of the global system is simulated in MATLAB/ Simulink interface programming while the practical data are collected from an experimental model consisting of DFIG-WT to validate the effectiveness of the FRT control system. The numerical results have demonstrated the validity and robustness of the analytical stability argument using Lyapunov method.

TABLE 2. System parameters of the proposed hybrid wind farm.

Parameters	Values
(a) WT	
Optimal tip speed ratio	8.1
Maximum power coefficient	0.48
Cut in wind speed	3.5 m/s
Cut out wind speed	25 m/s
Rated wind speed	9 m/s
Air density	1.225 kg/m^3
(b) SCIG: Nordex (N43-600)	
Rated power	600 kW
Rated frequency	50 Hz
Rated voltage	690 v
Stator resistance Rs	0.0092 Ω
Stator leakage inductance Lls	0.1686 H
Rotor resistance Rr	0.0121 Ω
Rotor leakage inductance Llr	0.1446 H
Mutual inductance Lm	5.68 p.u
Number of pole pairs	2
(c) DFIG: Gamesa (G52-850)	
Rated power	850 kW
Rated frequency	50 Hz
Rated voltage	690 V
Stator resistance Rs	0.00332 Ω
Stator leakage inductance Lls	0.00649 H
Rotor resistance Rr	0.00278 Ω
Rotor leakage inductance Llr	0.00652 H
Mutual inductance	2.9 H
Number of poles	2
Nominal DC-bus voltage	1150 V
DC link capacitance	60 mF
Filter impedance	0.003+J 0.3 p.u
(d) Transformers	
Wind turbine tr.: Turns ratio	690 V/22 kV
Resistance	0.0081 pu
Reactance	0.0453 pu
substation tr.: Turns ratio	22 kV/220 kV
Resistance	0.0051 pu
Reactance	0.065 pu
(e) Grid parameters	
Grid voltage	220 kV
Grid frequency	50 Hz
S.C level	1000 MVA
X/R	8
(f) Transmission lines parameters	
Positive sequence resistance	0.1153 Ω/km
Zero sequence resistance	0.413 Ω/km
Positive sequence inductance	1.05 mH/km
Zero sequence inductance	2.7 mH/km
Positive sequence capacitance	11.33 nF /km
Zero sequence capacitance	5.01 nF /km

APPENDIX A
SYSTEM PARAMETERS

The system parameters are shown in Table 2.

APPENDIX B
WT MODELING

The mechanical power P_m extracted by the WT is described by

$$P_m = \frac{1}{2}.\rho.A.V_w^3.C_P(\lambda, \beta) \tag{B.1}$$

where ρ, A and V_w are air density, rotor swept area, and wind speed respectively. C_P is the power coefficient where β and λ are pitch angle and tip-speed ratio respectively. λ is given by:

$$\lambda = \frac{\omega_R R}{V_w} \tag{B.2}$$

where ω_R and R are the rotor speed and radius respectively.

Due to the existence of a gearbox with gear ratio n_g, the generator mechanical speed ω_r can be represented by:

$$\omega_r = n_g \omega_R \tag{B.3}$$

Also, the rotor mechanical torque is given by:

$$T_m = \frac{P_m}{\omega_r} \tag{B.4}$$

C_P can be described as a function of λ and β by the following the nonlinear equation [10]

$$C_p = 0.5176\left(\frac{116}{\lambda_i} - 0.4\beta - 5\right)e^{-\frac{21}{\lambda_i}} + 0.0068\lambda \tag{B.5}$$

$$\lambda_i = \left(\frac{1}{\lambda + 0.08\beta} - \frac{0.035}{\beta^3 + 1}\right)^{-1} \tag{B.6}$$

Fig. 15 illustrates the Cp-λ curves for different β. Based on Fig. 15 $Cp_{\_max} \approx 0.48$ at $\beta = 0°$ and $\lambda = \lambda_{opt} \approx 8.1$. The mechanical output power of WT is illustrated in Fig. 16. As described in Fig. 16 the maximum power point, for any specific wind speed occurred at optimum WT rotational speed.

REFERENCES

[1] Global Wind Energy Council (GWEC). (Apr. 2019). *Global Wind Report 2018*. [Online]. Available: http://www.gwec.net
[2] H. M. Fekry, A. A. Eldesouky, A. M. Kassem, and A. Y. Abdelaziz, "Power management strategy based on adaptive neuro fuzzy inference system for AC microgrid," *IEEE Access*, vol. 8, pp. 192087–192100, Oct. 2020.
[3] M. H. Qais, H. M. Hasanien, and S. Alghuwainem, "Output power smoothing of wind power plants using self-tuned controlled SMES units," *Electr. Power Syst. Res.*, vol. 178, Jan. 2020, Art. no. 106056.
[4] *VESTAS Wind Turbines Lifetime Extension*. Accessed: Mar. 30, 2021. [Online]. Available: https://shop.vestas.com/en/services/consultancy-and-training/vestas-lifetime-extension/
[5] *Siemens Gamesa Wind Turbines Lifetime Extension*. Accessed: Mar. 30, 2021. [Online]. Available: https://www.siemensgamesa.com/products-and-services/service-wind/life-extension/
[6] A. M. Rauf, V. Khadkikar, and M. S. E. Moursi, "A new fault ride-through (FRT) topology for induction generator based wind energy conversion systems," *IEEE Trans. Power Del.*, vol. 34, no. 3, pp. 1129–1137, Jun. 2019.
[7] A. Moghadasi, A. Sarwat, and J. M. Guerrero, "A comprehensive review of low-voltage-ride-through methods for fixed-speed wind power generators," *Renew. Sustain. Energy Rev.*, vol. 55, pp. 823–839, Mar. 2016.
[8] J. Dixon, L. Moran, J. Rodriguez, and R. Domke, "Reactive power compensation technologies: State-of-the-art review," *Proc. IEEE*, vol. 93, no. 12, pp. 2144–2164, Dec. 2005.
[9] A. Rashad, S. Kamel, and F. Jurado, "Stability improvement of power systems connected with developed wind farms using SSSC controller," *Ain Shams Eng. J.*, vol. 9, no. 4, pp. 2767–2779, Dec. 2018.
[10] A. A. Hussein and M. H. Ali, "Comparison among series compensators for fault ride through capability enhancement of wind generator systems," *Int. J. Renew. Energy Res.*, vol. 4, no. 3, pp. 767–776, 2014.
[11] A. M. Howlader and T. Senjyu, "A comprehensive review of low voltage ride through capability strategies for the wind energy conversion systems," *Renew. Sustain. Energy Rev.*, vol. 56, pp. 643–658, Apr. 2016.
[12] A. R. A. Jerin, P. Kaliannan, U. Subramaniam, and M. S. E. Moursi, "Review on FRT solutions for improving transient stability in DFIGWTs," *IET Renew. Power Gener.*, vol. 12, no. 15, pp. 1786–1799, 2018.
[13] I. Ngamroo, "Review of DFIG wind turbine impact on power system dynamic performances," *IEEJ Trans. Electr. Electron. Eng.*, vol. 12, no. 3, pp. 301–311, May 2017.

[14] B. Shakerighadi, E. Ebrahimzadeh, F. Blaabjerg, and C. L. Bak, "Large-signal stability modeling for the grid-connected VSC based on the Lyapunov method," *Energies*, vol. 11, no. 10, p. 2533, Sep. 2018.
[15] L. Sun, B. Xu, W. Du, and H. Wang, "Model development and small-signal stability analysis of DFIG with stator winding inter-turn fault," *IET Renew. Power Gener.*, vol. 11, no. 3, pp. 338–346, Feb. 2017.
[16] A. Bennouk, A. Nejmi, and M. Ramzi, "Stability enhancement of a wind plant based on a DFIG and a PMSM: A Lyapunov approach," *Energy Rep.*, vol. 4, pp. 13–22, Nov. 2018.
[17] Y. Mishra, S. Mishra, F. Li, Z. Y. Dong, and R. C. Bansal, "Small-signal stability analysis of a DFIG-based wind power system under different modes of operation," *IEEE Trans. Energy Convers.*, vol. 24, no. 4, pp. 972–982, Dec. 2009.
[18] M. Li, W. Huang, N. Tai, and M. Yu, "Lyapunov-based large signal stability assessment for VSG controlled inverter-interfaced distributed generators," *Energies*, vol. 11, no. 9, p. 2273, Aug. 2018.
[19] P. Chen, D. Han, and K.-C. Li, "Robust adaptive control of maximum power point tracking for wind power system," *IEEE Access*, vol. 8, pp. 214538–214550, Nov. 2020.
[20] N. Ullah, I. Sami, M. S. Chowdhury, K. Techato, and H. I. Alkhammash, "Artificial intelligence integrated fractional order control of doubly fed induction generator-based wind energy system," *IEEE Access*, vol. 9, pp. 5734–5748, Dec. 2021.
[21] A. F. Tazay, A. M. A. Ibrahim, O. Noureldeen, and I. Hamdan, "Modeling, control, and performance evaluation of grid-tied hybrid PV/wind power generation system: Case study of Gabel El-Zeit region, Egypt," *IEEE Access*, vol. 8, pp. 96528–96542, Jun. 2020.
[22] L. A. E. K. Saleh, "Impact of the integration of the 63 MW wind-farm in Zafarana Egypt on the unified power-grid," *Appl. Energy*, vol. 74, nos. 1–2, pp. 247–260, Jan. 2003.
[23] A. M. Amin, M. M. A. Mahfouz, and B. E. Youssef, "Improvement integration of Zafrana Egypt wind farm connected to the unified power grid," *Int. Elect. Eng. J.*, vol. 1, no. 1, pp. 514–522, 2011.
[24] A. H. Kasem, E. F. El-Saadany, H. H. El-Tamaly, and M. A. A. Wahab, "An improved fault ride-through strategy for doubly fed induction generator-based wind turbines," *IET Renew. Power Gener.*, vol. 2, no. 4, pp. 201–214, Dec. 2008.
[25] M. K. Hossain and M. H. Ali, "Transient stability augmentation of PV/DFIG/SG-based hybrid power system by parallel-resonance bridge fault current limiter," *Electr. Power Syst. Res.*, vol. 130, pp. 89–102, Jan. 2016.
[26] R. Ruiz-Cruz, E. N. Sanchez, A. G. Loukianov, and J. A. Ruz-Hernandez, "Real-time neural inverse optimal control for a wind generator," *IEEE Trans. Sustain. Energy*, vol. 10, no. 3, pp. 1172–1183, Jul. 2019.
[27] A. Tanvir, A. Merabet, and R. Beguenane, "Real-time control of active and reactive power for doubly fed induction generator (DFIG)-based wind energy conversion system," *Energies*, vol. 8, no. 9, pp. 10389–10408, Sep. 2015.
[28] R. Hiremath and T. Moger, "Comprehensive review on low voltage ride through capability of wind turbine generators," *Int. Trans. Electr. Energy Syst.*, vol. 30, no. 10, Oct. 2020, Art. no. e12524.
[29] O. P. Mahela, N. Gupta, M. Khosravy, and N. Patel, "Comprehensive overview of low voltage ride through methods of grid integrated wind generator," *IEEE Access*, vol. 7, pp. 99299–99326, 2019.
[30] S. I. Gkavanoudis and C. S. Demoulias, "Fault ride-through capability of a DFIG in isolated grids employing DVR and supercapacitor energy storage," *Int. J. Electr. Power Energy Syst.*, vol. 68, pp. 356–363, Jun. 2015.
[31] *Wind Farm Grid Connection Code in addition to the Egyptian Transmission Grid Code (ETGC) Egyptian Distribution Network*. Egypt ERA Committee, Cairo, Egypt. Accessed: Mar. 2014. [Online]. Available: https://www.eehc.gov.eg/eehcportalnew/NewEnergyPDF/Egypt_gridcode_for_wind_farm_connection.pdf
[32] E. N. On, "Grid code regulations for high and extra high voltage," Netz Gmbh, Hohenahr, Germany, Tech. Rep. ENENARHS2006, Apr. 2006.
[33] M. Q. Duong, G. N. Sava, F. Grimaccia, S. Leva, M. Mussetta, S. Costinas, and N. Golovanov, "Improved LVRT based on coordination control of active crowbar and reactive power for doubly fed induction generators," in *Proc. 9th Int. Symp. Adv. Topics Electr. Eng.*, May 2015, pp. 650–655.
[34] S. H. A. Aleem, A. Y. Abdelaziz, and A. F. Zobaa, "Egyptian grid code of wind farms and power quality," in *Handbook of Distributed Generation*, Cham, Switzerland: Springer, 2017, pp. 227–245.
[35] B. Weise, "Impact of K-factor and active current reduction during fault-ride-through of generating units connected via voltage-sourced converters on power system stability," *IET Renew. Power Gener.*, vol. 9, no. 1, pp. 25–36, Jan. 2015.
[36] K. E. Okedu, S. M. Muyeen, R. Takahashi, and J. Tamura, "Wind farms fault ride through using DFIG with new protection scheme," *IEEE Trans. Sustain. Energy*, vol. 3, no. 2, pp. 242–254, Apr. 2012.
[37] J. Chiasson, *Modeling and High-Performance Control of Electric Machines*, Hoboken, NJ, USA: Wiley, 2005.
[38] A. Oteafy and J. Chiasson, "A study of the Lyapunov stability of an open-loop induction machine," *IEEE Trans. Control Syst. Technol.*, vol. 18, no. 6, pp. 1469–1476, Nov. 2010.
[39] M. Hinkkanen, L. Tiitinen, E. Molsa, and L. Harnefors, "On the stability of volts-per-hertz control for induction motors," *IEEE J. Emerg. Sel. Topics Power Electron.*, early access, Feb. 19, 2021, doi: 10.1109/JESTPE.2021.3060583.
[40] H. K. Khalil, *Nonlinear Systems*, 3rd ed. Englewood Cliffs, NJ, USA: Prentice-Hall, 2002.

AHMED A. SALEM received the B.Sc. degree in electrical engineering from Suez Canal University, Ismailia, Egypt, in 2004, the M.Sc. degree in electrical engineering from Port Said University, Egypt, in 2012, and the Ph.D. degree in electrical engineering from Suez Canal University, in 2017. He is currently working as an Assistant Professor with the Department of Electrical Engineering, Faculty of Engineering, Suez Canal University. His research interests include micro-grid control and operation and renewable energy based distribution systems with emphasis on smart grid application.

AZZA A. ELDESOUKY received the B.Sc. and M.Sc. degrees in electrical engineering from Suez Canal University, Port Said, in 1989 and 1995, respectively, and the Ph.D. degree from the University of Bath, U.K., in 2002. She is currently working as a Professor with the Department of Electrical Engineering, Port Said University. Her research interests include power system operation and management, power quality, micro-grid stability and control, smart grids, distributed generation, and AI applications in energy systems.

AHMED A. FARAHAT received the B.Sc. degree in electrical engineering from Alexandria University, Egypt, in 2011, and the M.Sc. degree in electrical engineering from Port Said University, Port Said, Egypt, in 2018. He is currently working as an Electrical Engineer with Damietta Power Station, Egypt.

ABDELAZEEM A. ABDELSALAM (Member, IEEE) received the B.Sc., M.Sc., and Ph.D. degrees in electrical engineering from Suez Canal University, Egypt, in 2001, 2005, and 2011, respectively. He was a Postdoctoral Fellow with the University of Ontario Institute of Technology (UOIT), Canada. He is currently working as an Associate Professor with Suez Canal University. His research interests include power quality, D-FACTS technology, switched filter compensators, micro-grid interface and control, and application of artificial intelligence techniques in power systems.